



Passive sampling of nonpolar contaminants at three deep-ocean sites



Kees Booij*, Ronald van Bommel, Hendrik M. van Aken, Hans van Haren, Geert-Jan A. Brummer, Herman Ridderinkhof

NIOZ Royal Netherlands Institute for Sea Research, P.O. Box 59, 1790 AB, Texel, The Netherlands

ARTICLE INFO

Article history:

Received 12 May 2014

Received in revised form

30 July 2014

Accepted 11 August 2014

Available online

Keywords:

Passive sampling

Nonpolar contaminants

Deep ocean

Performance reference compounds

Semipermeable membrane devices

ABSTRACT

Concentrations of polychlorinated biphenyls, polyaromatic hydrocarbons, hexachlorobenzene, and DDE were determined by passive sampling (semipermeable membrane devices) with exposure times of 1–1.5 years at 0.1–5 km depth in the Irminger Sea, the Canary Basin (both North Atlantic Ocean), and the Mozambique Channel (Indian Ocean). The dissipation of performance reference compounds revealed a pronounced effect of hydrostatic pressure on the sampler–water partition coefficients. Concentrations in the Irminger Sea were uniform over the entire water column (0.1–3 km). At the Canary Basin site, concentrations were 2–25 times lower near the bottom (5 km) than at 1.4 km. Concentrations in the Mozambique Channel (0.6–2.5 km) were lower than at the other two locations, and showed a near-bottom maximum. The data suggest that advection of surface waters down to a depth of about 1 km is an important mechanism of contaminant transport into the deep ocean.

© 2014 Elsevier Ltd. All rights reserved.

1. Introduction

Little data is available to assess the role of the deep ocean in the global fate of organic contaminants. Transport models consider the water below the surface mixed layer to be unimportant for atmosphere–water and meridional transport of organics (Semeena and Lammel, 2003; Gouin and Wania, 2007). Transport from the surface mixed layer to the deep ocean by vertical advection and particle settling is generally considered to be small or negligible on the time scale of decades (Wania and Mackay, 1995; Gouin and Wania, 2007). By contrast, Gustafsson et al. (1997) argue that transport rates of polychlorinated biphenyls (PCBs) to the deep North Atlantic Ocean are larger than atmospheric photo-degradation rates of these compounds, and a modelling approach by Scheringer et al. (2004) suggested that deposition to the deep ocean retards the long range transport of the heavier PCBs. Lohmann et al. (2006) estimate that PCB transport by deep convection is more important locally than particle mediated transport in the Norwegian Sea, Labrador Sea, Weddell Sea, and Ross Sea.

Transport to the deep ocean has been demonstrated using sediment trap data (Knap et al., 1986; Gustafsson et al., 1997; Dachs et al., 1999; Bouloubassi et al., 2006). Dissolved and particulate PCBs have been determined using in situ filtration/extraction of

deep waters in the North Atlantic Ocean, near the South-Western edge of the Porcupine Abyssal Plain (47°N 20°W) (Schulz et al., 1988). Similar measurements have been made for PCBs and PAHs around Iceland (Schulz-Bull et al., 1998). Passive sampling methods have been widely used for determining concentrations of freely dissolved nonpolar contaminants in surface waters (Stuer-Lauridsen, 2005; Greenwood et al., 2007; Allan et al., 2009), but not in the deep ocean. Lohmann and Muir (2010) recognised the potential of passive samplers for monitoring nonpolar contaminants around the globe, including the open ocean. The increased use of bottom landers and semi-permanent moorings for long-term monitoring of ocean current velocities, sedimentation, temperature, and salinity, among others, offers opportunities to collect contaminant concentration data in the deep ocean, at a small additional cost. Such data may be complementary to concentration data obtained by large-volume filtration/extraction methods. The latter methods are labour intensive, requiring the filtration and extraction of several hundred up to one thousand litres of water, and extreme care in controlling the blank levels (Schulz-Bull et al., 1998; Sobek and Gustafsson, 2004), but their application is not confined to specific mooring locations. Passive sampling methods are technically less complicated, but require attachment to a mooring or lander, and long exposure times are needed to extract sufficiently large volumes of water (400–1000 L), e.g., several months, up to one year, at equivalent water sampling rates of several litres per day. Further, passive samplers yield estimates of time-averaged concentrations of freely dissolved compounds,

* Corresponding author.

E-mail address: kees.booi@nioz.nl (K. Booij).

whereas filtration extraction methods yield the instantaneous concentrations of freely dissolved plus colloiddally bound compounds.

The aim of this study was to assess the potential of passive sampling to determine aqueous concentrations of nonpolar contaminants at deep ocean sites.

2. Methods

2.1. Passive samplers

Semipermeable membrane devices (SPMDs) were constructed using low-density polyethylene (LDPE) lay-flat tubing (2.54 cm wide, wall thickness 112 μm , Brentwood Plastics Inc., St. Louis, MO, USA) and triolein (99% purity, Sigma–Aldrich), following methods described previously (Booij et al., 2006). The SPMD dimensions were: length 64.9 ± 0.6 cm, mass 0.0039 ± 0.0001 kg, surface area 330 ± 3 cm². The triolein mass fraction was 0.166 ± 0.004 , which is somewhat smaller than the recommended value of 0.20 (p. 186 of Huckins et al., 2006), but this only has a marginal effect (<11%) on the SPMD-water partition coefficients (Supplementary data, S1). The triolein was spiked with performance reference compounds (PRCs) prior to construction of the SPMDs: 410 ng g⁻¹ acenaphthene-*d*₁₀, PCB4, phenanthrene-*d*₁₀, fluoranthene-*d*₁₀, and chrysene-*d*₁₂, and 15 ng g⁻¹ PCB29, PCB155, and PCB204. After construction, SPMDs were stored at -20 °C in separate hexane rinsed glass jars with lids that were lined with hexane-rinsed aluminium foil.

Exposure cages consisted of 7 titanium rods (5 mm diameter), clamped between two poly(oxyethylene) plates (2 cm thickness) that also supported a titanium or anodised aluminium mesh screen (1.5 × 1.5 cm openings) (Supplementary data, S2).

Before each deployment cruise, the SPMDs were mounted in the cages at the laboratory, with the exception of the deployments in the Mozambique Channel, for which the samplers were mounted in the cages on board of the ship, for logistic reasons. The cages were wrapped in aluminium foil and transferred to 22 × 50 cm air tight tins that were transported to the ships on dry ice and kept at -20 °C shipboard. About one hour before deployment, the tins were brought on deck. Immediately before deployment, the tins were opened, the cages were mounted on the mooring cable with four bolts (Supplementary data, S2), and the aluminium foil wrappings were removed. Upon recovery of the mooring, the cages were removed from the cable, transferred to the tins, and stored at -20 °C, as quickly as possible (15–30 min), to minimise exposure to the atmosphere on deck. Field control samplers received the same treatment as the deployed samplers, except for the actual deployment. Fabrication control samplers were kept frozen in the laboratory.

After recovery, the surfaces of the SPMDs were cleaned with a damp paper tissue to remove the biofilm. Only a faint brown colour was visible on the paper tissues, indicating minimal fouling. Only one SPMD (Mozambique Channel, 100 m) was damaged during the exposures, showing that the samplers had sufficient strength for a 1 to 1.5 y exposure in the deep ocean. SPMDs were extracted twice (16 h + 24 h) with 200 mL pentane. Internal standards (PCB112, PCB198, anthracene-*d*₁₀, pyrene-*d*₁₀, benzo[*a*]anthracene-*d*₁₂, perylene-*d*₁₂, indeno[1,2,3-*cd*]pyrene-*d*₁₂) were added at the beginning of the first extraction. The concentrated extracts were cleaned-up with silica (2 g, deactivated with 6% water, elution with pentane), and were analysed by GC-ECD for HCB, 4,4'-DDE, PCBs) and by GC-MS for PCB4 and PAHs with 3–6 aromatic rings (Supplementary data, S4).

Recoveries, determined from spiked SPMDs, were $102 \pm 12\%$ for PAHs and $100 \pm 9\%$ for HCB/DDE/PCBs. Contaminant levels in the solvent blanks were 4 ng for phenanthrene, 0.2 ng for the other PAHs, and 0.04 ng for the chlorinated compounds. The amounts in the fabrication control samplers were higher: 11 ng for phenanthrene, 3 ng for fluoranthene, 1 ng for pyrene, 0.5 ng for the other PAHs, and 0.2 ng for the chlorinated compounds. Contaminant levels in the field control samplers were higher than in the fabrication controls by a factor of about 2 for the PAHs and the di-, tri-, and tetrachlorobiphenyls. No differences between field controls and fabrication controls were observed for DDE, HCB, and the higher chlorinated PCBs. Detection limits (LOD) were calculated as the average plus three times the standard deviation of the amounts that were detected in the field controls. The average amounts in the field controls were subtracted from the amounts detected in the exposed samplers. A comparison of amounts detected in solvent blanks, fabrication controls, field controls, and a typical exposed SPMD is given in the Supplementary data (S3).

SPMD-water partition coefficients (K_{sw}) (L kg⁻¹) were calculated from

$$\log K_{sw} = 0.885 \log K_{PE-w} + 0.88 + K_s I \quad (1)$$

$s = 0.17, R^2 = 0.98$

$$\log K_{sw} = 1.057 \log K_{ow} - 0.45 + K_s I \quad (2)$$

$s = 0.30, R^2 = 0.95$

where $\log K_{PE-w}$ is the LDPE-water partition coefficient, K_s is the Setschenow constant (L mol⁻¹), used to adjust the partition coefficients for salinity, and I is the ionic strength of the water. These correlations were based on measured and calculated K_{sw} values as outlined in the Supplementary data (S5). Eq. (2) is less accurate

(standard error of 0.30 vs. 0.17), but can be used when $\log K_{PE-w}$ is not available. A K_s value of 0.35 L mol⁻¹ was adopted for all analytes (Jonker and Muijs, 2010).

It was assumed (and verified below; Section 3.1) that equilibrium was attained for all compounds with membrane-controlled uptake rates. Hence, only water boundary layer-controlled sampling rates need to be considered. These can be modelled as (Huckins et al., 2006; Booij and Smedes, 2010)

$$R_s = \beta_V V_m^{-0.39} \quad (3)$$

where V_m is the molar volume (reflecting compound-specific effects on R_s) and β_V is a site-specific parameter. Sampling rates (R_s) were obtained by unweighted nonlinear least squares estimation (Booij and Smedes, 2010) by fitting the retained PRC fractions (f) as a function of $K_{sw} V_m^{0.39}$.

$$f = \exp\left(-\frac{R_s t}{K_{sw} m_s}\right) = \exp\left(-\frac{\beta_V t}{K_{sw} V_m^{0.39} m_s}\right) \quad (4)$$

where m_s is the sampler mass and t is time. Aqueous concentrations (C_w) were calculated from the absorbed amounts (N) using

$$C_w = \frac{N}{K_{sw} m_s \left[1 - \exp\left(-\frac{R_s t}{K_{sw} m_s}\right)\right]} = \frac{N}{K_{sw} m_s \left[1 - \exp\left(-\frac{\beta_V t}{K_{sw} V_m^{0.39} m_s}\right)\right]} \quad (5)$$

Selected values of V_m and $\log K_{sw}$ are listed in the Supplementary data (S4).

2.2. Study area

Deployments were made in the Irminger sea (59.1 °N, 35.7 °W), the Canary Basin (29.4 °N, 23.1 °W), and the Mozambique Channel (16.7 °S, 40.9 °E), at depths of 0.1–5.1 km below the surface, for periods of 343–584 days in the years 2003–2005. Area map, bottom topography, horizontal and vertical positions of the samplers, deployment times, and average current velocities, temperatures, and salinities are summarised in the Supplementary data (S6, S7, S8).

3. Results and discussion

3.1. Sampling rate estimation

Analysis of the residuals in the modelling of PRC retention (Eq. (4)) revealed systematic deviations. The mean of the residuals for each PRC (averaged over all exposures) should not be significantly different from zero if Eq. (4) is a valid model for PRC retention and if the K_{sw} values are correct. Instead, the observed retained fractions of PCB29 and PCB155 were significantly smaller than the modelled fractions, whereas the reverse was true for acenaphthene-*d*₁₀, phenanthrene-*d*₁₀, PCB4, fluoranthene-*d*₁₀ (Fig. 1). Residuals (observed – modelled) for PCB29 were negatively correlated with exposure depth ($p < 0.01$, Fig. 2) and positive correlations with depth were found for acenaphthene-*d*₁₀, phenanthrene-*d*₁₀, and fluoranthene-*d*₁₀ ($p < 0.001$) (Supplementary data, S9).

The origin of the depth dependency of the residuals is illustrated in Fig. 3 for the shallowest (0.1 km) and deepest (5.1 km) exposure site. Retention data for PCBs and PAHs follow distinct model lines, which are close together for shallow exposures but are increasingly separated at greater depth. When PCB and PAH data are modelled together (solid lines in Fig. 3), the difference between observed and modelled PCB29 retention increases from 0.1 at 100 m to 0.3 at 5.1 km. Because the uptake rates of PCBs and PAHs are controlled by the water boundary layer it is unlikely that these compound groups actually have different sampling rates. We therefore suggest that the differences in PRC retention as a function of $\log K_{ow}$ are caused by inaccuracies in the K_{sw} values of these compound groups. These differences cannot be explained by temperature differences between shallow (~11 °C) and deep waters (~1 °C). Booij et al. (2003) found no measurable effect of temperature on the K_{sw} of SPMDs for PAHs, hexachlorobenzene, and PCBs. Huckins et al. (2002) reported a 0.2 log units decrease in the K_{sw} per 10 °C temperature increase for phenanthrene, but not for PCB52 and 4,4'-DDE. The shift of the model curve for PCBs relative to PAHs (~0.8 log units, Fig. 3 right) is much larger than can be explained by temperature. We therefore hypothesize that these effects are mainly caused by

different pressure dependencies of K_{sw} for PCBs and PAHs. The effect of pressure on the solute partitioning between an organic solvent and water follows the relationship

$$\frac{\partial \ln K}{\partial p} = -\frac{V_o - V_w}{RT} \quad (6)$$

where K is the solvent-water partition coefficient, p is pressure, R is the gas constant, T is the absolute temperature, and V_o and V_w are the partial molar volumes of the solute in the organic solvent and in water. An increase of K with pressure is expected for solutes that have a smaller partial molar volume in the organic phase than in the water phase, i.e., higher pressures push solutes into the organic phase if this results in a volume decrease. Both the magnitude and the direction of the pressure effect are difficult to predict. Lohmann (2012) speculated that K_{sw} would decrease with increasing pressure due to a reduction of free volume in the LDPE polymer, but it should be noted that the pressure effect is in the first place caused by the solute's $V_o - V_w$, and that a pressure induced change in the properties of water and the organic phase is a secondary effect that may cause the $\log K_{sw} - p$ relationship to become nonlinear. This secondary effect is probably modest, because the compressibility of the phases is small ($\sim 5 \cdot 10^{-10} \text{ Pa}^{-1}$): a pressure of 50 MPa ($\sim 5 \text{ km}$ water) induces a volume reduction of only 2–3% for water (Chen and Millero, 1976), LDPE (Isacescu et al., 1971), and triolein (Kielczynski, 2010). Sawamura (2000) noted that hydrocarbon transfer from a nonpolar solvent to water generally is associated with a decrease in the solute's partial molar volume (i.e., $V_o - V_w > 0$), which would result in a decrease of K with increasing pressure. It can also be hypothesised that $V_o - V_w < 0$, because solutes may fill the cavities of the free volume in the organic phase. For LDPE these cavities have a radius of 0.2–0.3 nm (Dlubek et al., 1998; Osoba, 1999; Zhou et al., 2000), which is close to the molecular radius of PCBs and PAHs ($\sim 0.5 \text{ nm}$), and similar considerations may apply to triolein.

A 0.8 log units difference between the PRC retention curves for PCBs and PAHs at 50 MPa would imply a $85 \text{ cm}^3 \text{ mol}^{-1}$ difference in $V_o - V_w$ between these PRC groups, which is large compared with the molar volumes of these compounds (e.g., $251 \text{ cm}^3 \text{ mol}^{-1}$ for chrysene and $247 \text{ cm}^3 \text{ mol}^{-1}$ for PCB29). Further study on the

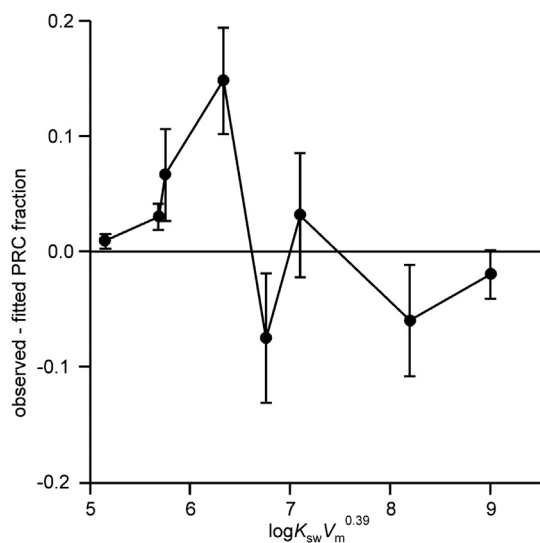


Fig. 1. Residuals in the retained PRC fractions as a function $\log K_{sw} V_m^{0.39}$ (Eq. (4)). Error bars span the 95% confidence ranges of the means. PRCs are from left to right: acenaphthene- d_{10} , phenanthrene- d_{10} , PCB4, fluoranthene- d_{10} , PCB29, chrysene- d_{12} , PCB155, PCB204.

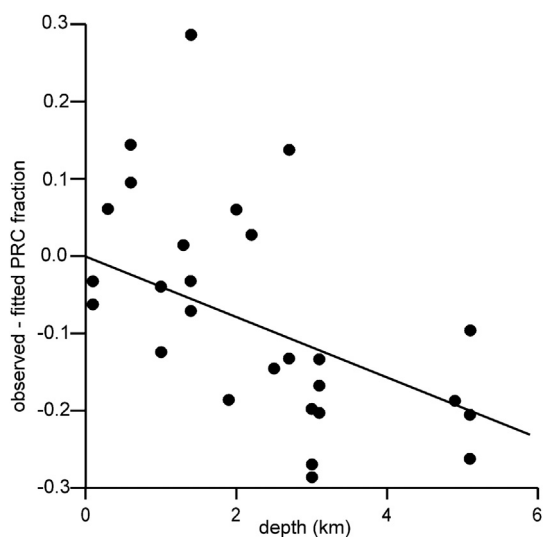


Fig. 2. Residuals in the retained fractions of PCB29 as a function of exposure depth.

pressure dependency of sampler-water partition coefficients is needed. The present data on PRC retention only suggests that the pressure dependency of K_{sw} is different for PCBs and PAHs, but the direction and magnitude of this effect are unknown. We therefore decided to use all PRCs and apply no pressure correction on K_{sw} . This implies that there could be a depth-dependent error in the estimated R_s (next paragraph).

Sampling rates of pyrene ($V_m = 214 \text{ cm}^3 \text{ mol}^{-1}$) ranged from 2 to 14 L d^{-1} and showed no significant increase with increasing current speed (Supplementary data, S10). The average pyrene R_s , taken over all exposures, was 6.9 L d^{-1} , with a standard error of 2.9 L d^{-1} ($\sim 42\%$). The standard error in $\log R_s$ was 0.19. Compounds with $\log K_{ow} > 5.8$ typically attained $< 50\%$ sampler-water equilibrium. This means that all compounds with membrane-controlled uptake kinetics ($\log K_{ow} < 4.5$) had attained their equilibrium concentrations, and that the selected R_s model (Eq. (3)) applies. The total uncertainty in the C_w estimates for compounds that reached equilibrium mainly depends on the errors in K_{sw} : 0.17 log units for near-surface exposures (Eq. (1)) plus an error that increases with depth, due to the effect of pressure on K_{sw} . The latter error is difficult to quantify, but we suggest to adopt a value of 0.4 log units at 5 km, i.e., half of the hypothesised 0.8 log units difference between the PRC retention curves for PAHs and PCBs. The total error is then expected to increase from 0.2 log units for near-surface deployments to 0.6 log units at 5 km. Uncertainties in the C_w of compounds that remain in the kinetic sampling stage only depend on the errors in R_s , which in turn depend on the errors in the K_{sw} of the PRCs, i.e., again 0.2 log units (factor of 1.6) for near-surface exposures, increasing to 0.6 log units (factor of 4) at 5 km.

3.2. Aqueous concentrations

Hexachlorobenzene and 4,4'-DDE were detected at all locations (LOD = 0.04 and 0.01 pg L^{-1} , respectively). Detection of PAHs and PCBs was limited to the compounds with higher molecular weight (PAHs with 4–6 aromatic rings, and PCBs with 5–8 chlorine atoms). The detection limits (ng L^{-1}) of the compounds with lower molecular weight were higher than those of the heavier compounds due to the higher amounts measured in the field controls (contamination during sampler fabrication, transport, and deployment/retrieval operations) and the fact that the effectively extracted water volume was limited by equilibrium attainment for

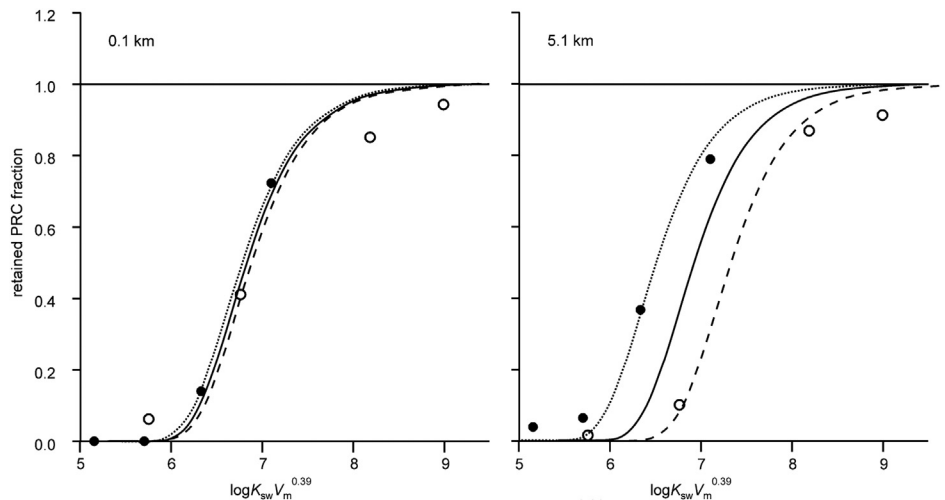


Fig. 3. Retained PRC fractions as a function of $\log K_{sw} V_m^{0.39}$ for the shallowest (left) and deepest (right) exposure sites. PCBs are shown as circles and deuterated PAHs as dots. Model fits (Eq. (4)) are shown for PCBs (dashed lines), deuterated PAHs (dotted lines) and all PRCs (solid lines).

these compounds, e.g., 170 L for phenanthrene (equilibrium sampling stage), versus 2–3 m³ for chrysene (kinetic sampling stage). A stricter control of fabrication and field blanks is needed to lower the LODs of the lighter compounds. The most frequently detected compounds were fluoranthene (93%), chrysene (100%), PCB151 (74%), PCB153 (70%). All concentrations are listed in the [Supplementary data \(S11, S12\)](#), together with the LODs. The vertical distributions of all PAHs were very similar. For this reason, and to allow for a comparison with literature data, fluoranthene was selected as a model PAH in the discussion below. For the same reasons, PCB153 was selected as a model-PCB.

3.3. Comparison with literature values

Comparisons with literature data on concentrations of dissolved contaminants in remote areas are difficult because of the limited data that is available, and because of the many sources of variability involved in such comparisons. Even within the same water basin,

sampling locations of different studies may be thousands of kilometres apart, and concentrations may be subject to temporal variability on decadal, annual, and seasonal time scales. In polar areas, concentrations determined by filtration/extraction methods may be biased towards spring/summer values, because bad weather conditions and sea ice formation in autumn and winter may preclude sampling during these seasons. In addition, methodological factors may contribute to the variability among studies. [Sobek et al. \(2003\)](#) reported a (within method) sampling variability for dissolved PCBs in Baltic Sea water between 14 and 77%. To our knowledge, no laboratory performance studies exist for organic contaminants in water, but results from the QUASIMEME program for PAHs in sediment and biota indicate that interlaboratory variability increases with decreasing determinand concentrations, up to 100% ([Law et al., 2000](#)). Considering that extraction methods for water are complex when compared with sediments and biota, and that aqueous concentrations in the open ocean are very low, the

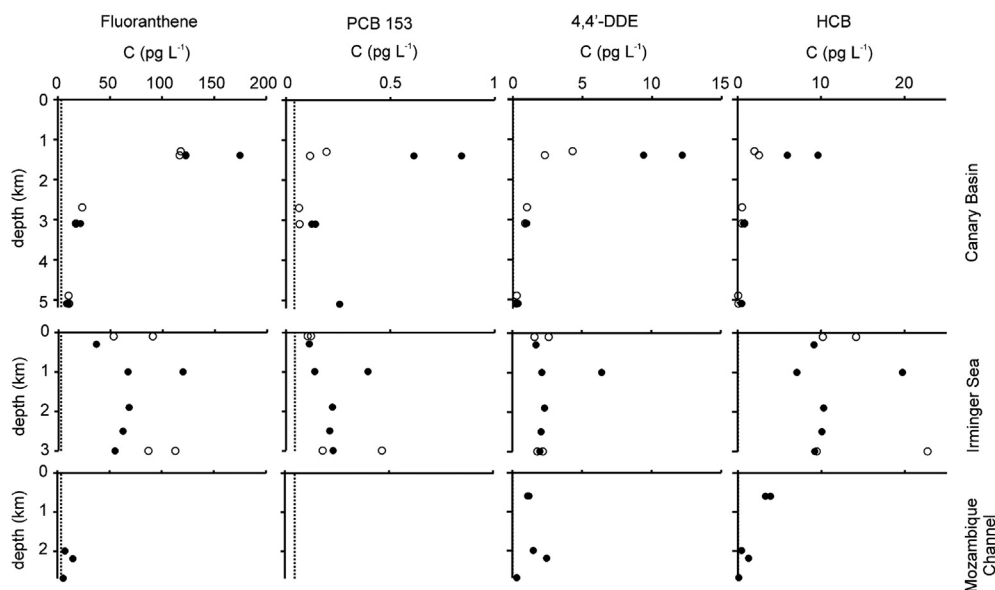


Fig. 4. Concentrations of fluoranthene, PCB153, 4,4'-DDE, and HCB in the Canary Basin (top, closed circles: 2003–2004, open circles 2004–2005), the Irminger Sea (middle, closed circles: 2003–2004, open circles 2005–2006), and the Mozambique Channel (bottom, 2003–2005). Dashed lines represent the detection limits. Vertical scales span the local water depth. Apparent duplicates (same depth, same period) actually represent exposures on different moorings ([Supplementary data, S6](#)).

interlaboratory variability in these data can be expected to be substantial, but as yet hard to quantify.

Passive sampling has its own unique features that should be kept in mind when comparing concentration measurements among different studies. First, passive samplers yield concentration estimates that are time integrated over a window of $\tau = K_{sw}m_s/R_s$. For the present study this amounts to about 0.5 y for fluoranthene, 1 y for HCB, 3 y for 4,4'-DDE and 3 decades for PCB153. By contrast, ship based filtration/extraction methods are time-integrative over the period of sample intake (~12 h). Uncertainties in passive sampling based aqueous concentrations strongly depend on the accuracy of the K_{sw} values of compounds that reach equilibrium during the exposure, and the K_{sw} values of PRCs for compounds that remain in the kinetic sampling stage. For the present study the errors in K_{sw} increase from 0.2 log units for near-surface exposures (factor of 1.6), to 0.6 log units (factor of 4) at 5 km (Section 3.1), and similar errors can be expected for the estimated C_w .

Bearing the above caveats in mind, the present concentration estimates compare well with literature values for the North Atlantic and Indian Ocean, but generally are at the high side of the spectrum (Table 1), particularly for 4,4'-DDE. A more detailed discussion is given in the Supplementary data (S13).

3.4. Canary Basin

Sampling sites were located on the eastern side of the North Atlantic Subtropical Gyre. The lower parts of the water column (>4 km) consist of Antarctic Bottom Water (AABW), which enters the eastern Atlantic basin via the Romanche and Vema Fracture Zones. Eurafican Mediterranean Water (EMW), found at 1–2 km (Tomczak and Godfrey, 2003), originates from the intermittent overflow at the Strait of Gibraltar followed by isopycnal spreading over the Atlantic Ocean with limited vertical mixing. The permanent thermocline is found at a depth of about 800 m (Johnson and Gruber, 2007) and the winter mixed layer depth is less than 150 m (van Aken, 2001). The upper parts of the water column consist of subtropical mode waters that are formed by cooling and subduction along the North Atlantic Current, followed by southward advection into the gyre's thermocline waters (Hanawa and Talley, 2001), and by Madeira Mode Water, which originates from the region north-west of the Canary Islands, and rapidly mixes with the thermocline waters of the gyre (Siedler et al., 1987; Hanawa and Talley, 2001).

Concentrations at 1.4 km are similar to literature values reported for surface waters (Table 1), suggesting that no large concentration gradients exist in the upper 1.4 km. Munk and Wunsch (1998) argue that an ocean-average vertical diffusivity of $D = 10^{-4} \text{ m}^2 \text{ s}^{-1}$ needs to be adopted in order to explain the existence of a stratified abyssal ocean. These authors hypothesise that most of the mixing originates from the dissipation of internal tides at continental margins, ocean ridges and seamounts, whereas mixing is less intense in areas away from these structures. Adopting this diffusivity results in a length scale ($L \approx \sqrt{Dt}$) of diffusional transport over a time period of one decade of 170 m, and a vertical diffusivity of $10^{-2} \text{ m}^2 \text{ s}^{-1}$ would be needed to explain the observed contaminant concentrations at 1.4 km. Although diffusivities up to $10^{-1} \text{ m}^2 \text{ s}^{-1}$ have been observed near topographic features (van Haren and Gostiaux, 2012), these are unlikely values at the Canary Basin sampling sites.

Particle mediated transport has been suggested as an important mechanism of contaminant transfer to the deep sea (Dachs et al., 2002; Bouloubassi et al., 2006). For an order-of-magnitude estimate of the significance of this mechanism, and neglecting the gradual depletion of the particles as a result of contaminant release to the surrounding waters, the organic carbon flux (j_{oc}) can conveniently be expressed as an equivalent downward water flow (u_w) by

Table 1

Comparison of concentrations of fluoranthene, PCB153, 4,4'-DDE, and hexachlorobenzene with literature values.

C (pg L ⁻¹)	Location	Source
Fluoranthene		
75	Irminger Sea	Present study
130	Canary Basin, 1.4 km	Present study
10	Canary Basin, 5.1 km	Present study
<3	Mozambique Channel, 0.6 km	Present study
9	Mozambique Channel, 2–2.7 km	Present study
110	East Atlantic (English Channel – equator)	Nizzetto et al. (2008)
50	East Atlantic (equator – Walvis Ridge)	Nizzetto et al. (2008)
20 – 190	Atlantic (Rhode Island – Equator)	Lohmann et al. (2013)
<11 – 50	Atlantic (Equator – Walvis Bay)	Lohmann et al. (2013)
<5 – 9	North Atlantic, 61–68 °N	Schulz-Bull et al. (1998)
20 – 130	Norwegian Sea	Lohmann et al. (2009)
10 – 50	Fram Strait (Greenland – Svalbard, 75–85 °N)	Lohmann et al. (2009)
PCB153		
0.2	Irminger Sea, 0.1–3 km	Present study
0.4	Canary Basin, 1.4 km	Present study
<0.04–0.3	Canary Basin, 5.1 km	Present study
<0.04	Mozambique Channel, 0.6 km	Present study
<0.04	Mozambique Channel, 2–2.7 km	Present study
0.05 – 0.2	East Atlantic	Gioia et al. (2008b)
<0.06	Atlantic (Rhode Island – Walvis Bay)	Lohmann et al. (2013)
0.3 – 2.7	Atlantic, (47°N, 20°W), 10–750 m	Schultz et al. (1988)
0.1	Atlantic, (47°N, 20°W), 3.5–4 km	
0.5 ^a	Atlantic (~30 °N)	Iwata et al. (1993)
0.02 – 0.06	North Atlantic, near Iceland, 61–68 °N	Schulz-Bull et al. (1998)
<0.01	Norwegian Sea	Gioia et al. (2008a)
<0.01	Fram Strait (Greenland-Svalbard, 75–85 °N)	Gioia et al. (2008a)
0.2–0.4 ^b	Norwegian Sea & Barents Sea 62–80 °N	Sobek and Gustafsson (2004)
0.01–0.2 ^b	Arctic 80–90 °N	Sobek and Gustafsson (2004)
0.1 – 0.2	Barents Sea near Svalbard	Gustafsson et al. (2005)
0.02 – 0.04	Arctic	Gustafsson et al. (2005)
0.2 – 0.8 ^a	Bay of Bengal, Arabian Sea	Iwata et al. (1993)
0.2 – 0.7 ^a	Eastern Indian Ocean	Iwata et al. (1993)
4,4'-DDE		
2.5	Irminger Sea, 0.1–3 km	Present study
7	Canary Basin, 1.4 km	Present study
0.3	Canary Basin, 5.1 km	Present study
1	Mozambique Channel, 0.6 km	Present study
1	Mozambique Channel, 2–2.7 km	Present study
0.5	Atlantic (~30 °N)	Iwata et al. (1993)
0.3 – 1.4	East Atlantic, northern hemisphere	Booij et al. (2007)
0.2 – 0.4	Norwegian Sea	Lohmann et al. (2009)
0.1 – 0.2	Greenland-Svalbard, 75–85 °N	Lohmann et al. (2009)
0.4 – 5	Bay of Bengal, Arabian Sea	Iwata et al. (1993)
0.8	Eastern Indian Ocean	Iwata et al. (1993)
HCB		
12	Irminger Sea, 0.1–3 km	Present study
5	Canary Basin, 1.4 km	Present study
0.3	Canary Basin, 5.1 km	Present study
4	Mozambique Channel, 0.6 km	Present study
0.6	Mozambique Channel, 2–2.7 km	Present study
0.1–3	Atlantic (Rhode Island – Equator)	Lohmann et al. (2012)
<0.2	Atlantic (Equator – Walvis Bay)	Lohmann et al. (2012)
2 – 9	East Atlantic, northern hemisphere	Booij et al. (2007)
3	East Atlantic, southern hemisphere	Booij et al. (2007)
1 – 2	Norwegian Sea	Lohmann et al. (2009)
2 – 10	Greenland-Svalbard, 75–85 °N	Lohmann et al. (2009)
7 – 19	Arctic	Barber et al. (2005)

^a Estimated from $\Sigma\text{PCB} = 26 \text{ pg L}^{-1}$ (Iwata et al., 1993) and a PCB153 mass fraction in $\Sigma_{29}\text{PCB}$ of 1.8% (Gioia et al., 2008b).

^b Concentrations of particulate + dissolved PCB153.

$$u_w = j_{oc} K_{oc} \quad (7)$$

where K_{oc} is the organic carbon to water partition coefficient. Adopting $j_{oc} = 1 \text{ g m}^{-2} \text{ y}^{-1}$ (Antia et al., 2001) yields $u_w = 0.1 \text{ m y}^{-1}$ at $\log K_{oc} = 5$ (e.g., fluoranthene) and 10 m y^{-1} at $\log K_{oc} = 7$ (e.g.,

PCB153), indicating that particle-associated transport is insignificant on decadal time scales.

Marti et al. (2001) observed concentrations of particle bound PAHs and PCBs in lenses of Euroafrican Mediterranean Water (EMW) north of Madeira at 800–1200 m, that were elevated relative to the surrounding North East Atlantic water by a factor of 1.2–2. Although EMW can be traced in the Atlantic Ocean over many thousands of kilometres, its relative contribution at the Canary Basin site is rather small. Using the average salinity of 35.3 at 1.4 km, and adopting an initial EMW salinity of 37.8 (Tomczak and Godfrey, 2003) and a background salinity of 34.9, results in an EMW content of about 14%. The small mass fraction of EMW and the small concentration differences that are observed between surface waters and overflow waters in Gibraltar Strait (Gomez, 2003) as well as the small concentration difference between EMW water lenses and Atlantic Water (Marti et al., 2001) make it unlikely that EMW significantly contributes to the contaminant signal at the Canary Basin site. Instead, we speculate that these concentrations originate from the advection of North Atlantic water that is entrained with the EMW during its overflow from the Strait of Gibraltar sill at ~300 m, and from the advection of subtropical mode waters formed in the southern edge of the North Atlantic Current. Additional measurements on a wider vertical and horizontal scale are needed to further test this hypothesis, however.

Concentrations decreased between 1.4 and 5 km by factors of ~10 (PAHs), 2 (PCBs), 25 (4,4'-DDE), and 16 (HCB) (Fig. 4), indicating limited vertical transport within this depth range. The low contaminant concentrations at 5 km can be understood from the presence of AABW, which has long been isolated from the atmosphere.

3.5. Irminger Sea

Contaminant concentrations at the Irminger Sea sites showed little variation over the depth range 0.1–3 km (Fig. 4), despite the widely different origin of the water masses. Sampling sites were located in the central and eastern side of the basin at about 59 °N, between Cape Farewell (Southern Greenland), and Reykjanes Ridge. The hydrology of the sub-surface Irminger Sea is dominated by Subpolar Mode Water (SPMW), Iceland Scotland Overflow Water (ISOW), Denmark Strait Overflow Water (DSOW), and Labrador Sea Water (LSW). Subpolar Mode Water, found in the upper few hundred metres in the Irminger Sea, is formed from the western branch of the North Atlantic Current, by deep winter convection (~400 m) in the Rockall Channel and the Iceland Basin, and is further advected into the Irminger Sea (McCartney and Talley, 1982) with the Irminger Current, which flows to the North at the western side of Reykjanes Ridge. Near the bottom (2.5–3 km), ISOW enters the Irminger Sea from the East, via the Charlie-Gibbs Fracture Zone where it continues as a counterclockwise circulation (van Aken, 2007). ISOW is formed in the Iceland Basin from the overflow of intermediate and deep waters in the Nordic seas that pass over the Iceland-Faroe-Scotland Ridge into the Iceland Basin, where they mix with Subpolar Mode Water and Labrador Sea Water (Fogelqvist et al., 2003; van Aken and de Jong, 2012). Near the Greenland slope, a southward flowing zone of DSOW is found at the bottom of the Irminger Sea. LSW, formed by deep convection in the Labrador Sea is found circulating counterclockwise above the ISOW (van Aken and de Jong, 2012) at a depth of 1–2 km (Fogelqvist et al., 2003). A different type of LSW is formed in the central Irminger Sea by deep winter convection down to 250–1000 m (de Jong et al., 2012).

The passive samplers in the Irminger Sea sites likely were exposed to LSW (100 and 300 m), SPMW (1 km), ISOW (below 1.9 km), and one of the samplers at 3 km may also have been affected by the eastern edge of the DSOW. These water masses

apparently have very similar contaminant concentrations, which either suggests that their source waters (at the sea surface) had similar concentrations, or that extensive mixing of the source waters with the surrounding waters occurred during their transport to the Irminger Sea. For example, Fogelqvist et al. (2003) conclude that the mass fraction of intermediate and deep water from the Norwegian Sea in ISOW, just south of the Iceland Scotland Ridge, is about 43%, and that ISOW further mixes with LSW during its passage through the Iceland Basin towards the Irminger Sea. Similarly, the SPMW is formed during deep winter convection over a large geographical area between the Rockall Channel and the Iceland Basin, and contaminant concentrations in SPMW thus reflect space averaged values of wintertime surface water concentrations. The emerging picture from the Irminger Sea sites is that there probably are no major differences in the contaminant concentrations at the formation sites of the water masses at the sampler exposure sites, i.e., Labrador Sea, Norwegian Sea, Greenland Sea, Iceland Basin, and North East Atlantic Ocean. By contrast, Schulz-Bull et al. (1998) observed a large decrease in concentrations of particle bound PAHs (eight-fold) and PCBs (seven-fold) in the central Irminger Sea between 50 and 2450 m. The occurrence of a vertical gradient observed by the latter authors may be due to the fact that sampling took place in August, when the central Irminger Sea is stratified. It should be noted however that the existence of an increase or decrease of concentrations with depth cannot be excluded in the present study due to the uncertainties in the sampling rates that result from the pressure dependency in the K_{sw} of the PRCs (Section 3.1). By the same reasoning as in Section 3.4, a vertical organic carbon flux of $0.6 \text{ g m}^{-2} \text{ y}^{-1}$ (Jonkers et al., 2010) does not significantly contribute to the contaminant flux.

3.6. Mozambique Channel

Contaminant concentrations at the Mozambique Channel sites were below or close to the detection limit, with the exception of HCB and 4,4'-DDE (Fig. 4). The hydrography of the Mozambique Channel is characterised by a southward flow of Tropical Surface Water, Subtropical Surface Water (upper 200 m), and South Indian Central Water (SICW, 200–600 m), and a northward flowing undercurrent consisting of Antarctic Intermediate Water (AAIW) and North Atlantic Deep Water (NADW), which is located along the western slope of the channel at a depth of 1.5–2.3 km (Ullgren et al., 2012). SICW is formed by subduction of Indian Ocean surface water at 40–45 °S (You, 1997). The upper 1.5 km of the Mozambique Channel is characterised by a high hydrographical variability associated with the southward passage of eddies, and current velocities ranging from a few cm s^{-1} in the deeper layers to several dm s^{-1} at the surface (Ullgren et al., 2012). The passive samplers likely were exposed to SICW (0.6 km) and NADW/AAIW (below 2 km). Fluoranthene concentrations were low (~9 pg L^{-1}) in the AAIW/NADW undercurrent, which is similar to the concentrations observed in AABW at the deep Canary Basin site. Fluoranthene concentrations were below detection in the SICW (0.6 km). Concentrations of PCB153 were below detection at all depths, reflecting the limited use of PCBs in the southern hemisphere. HCB concentrations at 0.6 km are somewhat lower than the concentrations in the Irminger Sea and in the Canary Basin (1.4 km), which is in line with the observation that concentrations of atmospheric HCB are somewhat lower in the southern hemisphere compared with the northern hemisphere (Barber et al., 2005). The concentrations of 4,4'-DDE in SICW are lower than the concentrations observed for the Canary Basin and the Irminger Sea, reflecting the low contamination levels in the Southern Indian Ocean (Iwata et al., 1993). The organic carbon flux of $2.6 \text{ g m}^{-2} \text{ y}^{-1}$ (Fallet et al., 2012) is the highest of the three locations but makes no

significant contribution to the vertical contaminant transport (Section 3.4).

4. Outlook

Valuable information can be obtained by passive sampling of nonpolar contaminants in the deep ocean. Two methodological difficulties need to be resolved for future application of this method. First, the pressure dependency of the sampler-water partition coefficients needs to be quantified and understood. Second, the contaminant levels in the field controls should be reduced. These levels prevented the detection of lower molecular weight analytes, such as PAHs with three aromatic rings and PCBs with less than five chlorine atoms.

Although we only studied three deep ocean sites, the evidence from ocean circulation studies combined with our concentration measurements suggest that vertical transport of contaminants is not limited to turbulent mixing in the ocean surface and deep convection in polar regions (Lohmann et al., 2006), but that advection of surface waters into the waters above the permanent thermocline in tropical, subtropical and subpolar regions should be considered as well.

Acknowledgements

The observations could be performed through collaboration with the Long term Ocean Climate Observation (LOCO) program and the Netherlands–Bremen Oceanography II (NEBROC2) program, funded by the Nederlandse Organisatie voor Wetenschappelijk Onderzoek (NWO). Crew and technical staff of the RV Pelagia (The Netherlands), the RV Darwin (UK), and the RV Discovery (UK) are acknowledged for their support in handling the moorings. Support of NIOZ-MTM is acknowledged.

Appendix A. Supplementary data

Supplementary data related to this article can be found at <http://dx.doi.org/10.1016/j.envpol.2014.08.013>.

References

- Allan, I.J., Booij, K., Paschke, A., Vrana, B., Mills, G.A., Greenwood, R., 2009. Field performance of seven passive sampling devices for monitoring of hydrophobic substances. *Environ. Sci. Technol.* 43, 5383–5390.
- Antia, A.N., Koeve, W., Fischer, G., Blanz, T., Schulz-Bull, D., Scholten, J., Neuer, S., Kremling, K., Kuss, J., Peinert, R., Hebbeln, D., Bathmann, U., Conte, M., Fehner, U., Zeitzschel, B., 2001. Basin-wide particulate carbon flux in the Atlantic Ocean: regional export patterns and potential for atmospheric CO₂ sequestration. *Glob. Biogeochem. Cycles* 15, 845–862.
- Barber, J.L., Sweetman, A.J., van Wijk, D., Jones, K.C., 2005. Hexachlorobenzene in the global environment: emissions, levels, distribution, trends and processes. *Sci. Total Environ.* 349, 1–44.
- Booij, K., Hofmans, H.E., Fischer, C.V., van Weerlee, E.M., 2003. Temperature-dependent uptake rates of non-polar organic compounds by semipermeable membrane devices and low-density polyethylene membranes. *Environ. Sci. Technol.* 37, 361–366.
- Booij, K., Smedes, F., 2010. An improved method for estimating in situ sampling rates of nonpolar passive samplers. *Environ. Sci. Technol.* 44, 6789–6794.
- Booij, K., van Bommel, R., Jones, K.C., Barber, J.L., 2007. Air-water distribution of hexachlorobenzene and 4,4'-DDE along a North-South Atlantic transect. *Mar. Pollut. Bull.* 54, 814–819.
- Booij, K., van Bommel, R., Mets, A., Dekker, R., 2006. Little effect of excessive biofouling on the uptake of organic contaminants by semipermeable membrane devices. *Chemosphere* 65, 2485–2492.
- Bouloubassi, I., Mejanelle, L., Pete, R., Fillaux, J., Lorre, A., Point, V., 2006. PAH transport by sinking particles in the open Mediterranean Sea: a 1 year sediment trap study. *Mar. Pollut. Bull.* 52, 560–571.
- Chen, C.T., Millero, F.J., 1976. Specific volume of seawater at high pressures. *Deep-Sea Res.* 23, 595–612.
- Dachs, J., Bayona, J.M., Ittekkot, V., Albaiges, J., 1999. Monsoon-driven vertical fluxes of organic pollutants in the western Arabian Sea. *Environ. Sci. Technol.* 33, 3949–3956.
- Dachs, J., Lohmann, R., Ockenden, W.A., Mejanelle, L., Eisenreich, S.J., Jones, K.C., 2002. Oceanic biogeochemical controls on global dynamics of persistent organic pollutants. *Environ. Sci. Technol.* 36, 4229–4237.
- de Jong, M.F., van Aken, H.M., Vage, K., Pickart, R.S., 2012. Convective mixing in the central Irminger Sea: 2002–2010. *Deep-Sea Res. Pt. I* 63, 36–51.
- Dlubek, G., Lupke, T., Fretwell, H.M., Alam, M.A., Wutzler, A., Radusch, H.J., 1998. The local free volume in deformed polyethylene: a positron lifetime study. *Acta Polym.* 49, 236–243.
- Fallet, U., Castaneda, I.S., Henry-Edwards, A., Richter, T.O., Boer, W., Schouten, S., Brummer, G.J., 2012. Sedimentation and burial of organic and inorganic temperature proxies in the Mozambique Channel, SW Indian Ocean. *Deep-Sea Res. Pt. I* 59, 37–53.
- Fogelqvist, E., Blindheim, J., Tanhua, T., Osterhus, S., Buch, E., Rey, F., 2003. Greenland-Scotland overflow studied by hydro-chemical multivariate analysis. *Deep-Sea Res. Pt. I* 50, 73–102.
- Gioia, R., Lohmann, R., Dachs, J., Temme, C., Lakašchus, S., Schulz-Bull, D., Hand, I., Jones, K.C., 2008a. Polychlorinated biphenyls in air and water of the North Atlantic and Arctic Ocean. *J. Geophys. Res. Atmos.* 113, D19302.
- Gioia, R., Nizzetto, L., Lohmann, R., Dachs, J., Temme, C., Jones, K.C., 2008b. Polychlorinated Biphenyls (PCBs) in air and seawater of the Atlantic Ocean: sources, trends and processes. *Environ. Sci. Technol.* 42, 1416–1422.
- Gomez, F., 2003. The role of the exchanges through the strait of Gibraltar on the budget of elements in the Western Mediterranean Sea: consequences of human-induced modifications. *Mar. Pollut. Bull.* 46, 685–694.
- Gouin, T., Wania, F., 2007. Time trends of arctic contamination in relation to emission history and chemical persistence and partitioning properties. *Environ. Sci. Technol.* 41, 5986–5992.
- Greenwood, R., Mills, G., Vrana, B., 2007. *Passive Sampling Techniques in Environmental Monitoring*. Elsevier, Amsterdam, pp. 1–453.
- Gustafsson, O., Andersson, P., Axelman, J., Bucheli, T.D., Komp, P., McLachlan, M.S., Sobek, A., Thorngren, J.O., 2005. Observations of the PCB distribution within and in-between ice, snow, ice-rafted debris, ice-interstitial water, and seawater in the Barents Sea marginal ice zone and the North Pole area. *Sci. Total Environ.* 342, 261–279.
- Gustafsson, O., Gschwend, P.M., Buesseler, K.O., 1997. Settling removal rates of PCBs into the Northwestern Atlantic derived from ²³⁸U–²³⁴Th disequilibria. *Environ. Sci. Technol.* 31, 3544–3550.
- Hanawa, K., Talley, L.D., 2001. Mode waters. Ch. 5.4. In: Siedler, G., Church, J., Gould, J. (Eds.), *Ocean Circulation and Climate*. Academic Press, San Diego, pp. 373–386.
- Huckins, J.N., Petty, J.D., Booij, K., 2006. *Monitors of Organic Chemicals in the Environment: Semipermeable Membrane Devices*. Springer, New York, pp. 1–223.
- Huckins, J.N., Petty, J.D., Lebo, J.A., Almeida, F.V., Booij, K., Alvarez, D.A., Cranor, W.L., Clark, R.C., Mogensen, B.B., 2002. Development of the permeability/performance reference compound approach for in situ calibration of semipermeable membrane devices. *Environ. Sci. Technol.* 36, 85–91.
- Isacescu, D.A., Ionescu, I.V., Leca, M., Roncea, C., Mihaita, D., Rizescu, E., 1971. Studies in the field of polyethylene-V. Correlations between compressibility, crystallinity and molecular weight of high pressure natural polyethylenes. *Eur. Polym. J.* 7, 913–932.
- Iwata, H., Tanabe, S., Sakai, N., Tatsukawa, R., 1993. Distribution of persistent organochlorines in the oceanic air and surface seawater and the role of ocean on their global transport and fate. *Environ. Sci. Technol.* 27, 1080–1098.
- Johnson, G.C., Gruber, N., 2007. Decadal water mass variations along 20°W in the Northeastern Atlantic Ocean. *Prog. Oceanogr.* 73, 277–295.
- Jonker, M.T.O., Muijs, B., 2010. Using solid phase micro extraction to determine salting-out (Setschenow) constants for hydrophobic organic chemicals. *Chemosphere* 80, 223–227.
- Jonkers, L., Brummer, G.J.A., Peeters, F.J.C., van Aken, H.M., de Jong, M.F., 2010. Seasonal stratification, shell flux, and oxygen inhibition dynamics of left-coiling *N. pachyderma* and *T. quinqueloba* in the western subpolar North Atlantic. *Paleoceanography* 25, PA2204.
- Kielczynski, P., 2010. Application of acoustic waves to investigate the physical properties of liquids at high pressure. Ch. 14. In: Dissanayake, D.W. (Ed.), *Acoustic Waves*, pp. 317–340. www.intechopen.com/books/acoustic-waves.
- Knap, A.H., Binkley, K.S., Deuser, W.G., 1986. Synthetic organic chemicals in the deep Sargasso Sea. *Nature* 319, 572–574.
- Law, R.J., Kelly, C.A., Nicholson, M.D., 2000. The QUASIMEME laboratory performance study of polycyclic aromatic hydrocarbons (PAHs): Assessment for the period 1996–1999. *J. Environ. Monit.* 2, 517–523.
- Lohmann, R., 2012. Critical review of low-density polyethylene's partitioning and diffusion coefficients for trace organic contaminants and implications for its use as a passive sampler. *Environ. Sci. Technol.* 46, 606–618.
- Lohmann, R., Gioia, R., Jones, K.C., Nizzetto, L., Temme, C., Xie, Z., Schulz-Bull, D., Hand, I., Morgan, E., Jantunen, L., 2009. Organochlorine pesticides and PAHs in the surface water and atmosphere of the North Atlantic and Arctic Ocean. *Environ. Sci. Technol.* 43, 5633–5639.
- Lohmann, R., Jurado, E., Pilon, M.E.Q., Dachs, J., 2006. Oceanic deep water formation as a sink of persistent organic pollutants. *Geophys. Res. Lett.* 33, Article L12607.
- Lohmann, R., Klanova, J., Kukucka, P., Yonis, S., Bollinger, K., 2012. PCBs and OCPs on a East-to-West transect: the importance of major currents and net volatilization for PCBs in the Atlantic Ocean. *Environ. Sci. Technol.* 46, 10471–10479.
- Lohmann, R., Klanova, J., Pribylova, P., Liskova, H., Yonis, S., Bollinger, K., 2013. PAHs on a West-to-East transect across the tropical Atlantic Ocean. *Environ. Sci. Technol.* 47, 2570–2578.

- Lohmann, R., Muir, D., 2010. Global aquatic passive sampling (AQUA-GAPS): using passive samplers to monitor POPs in the waters of the world. *Environ. Sci. Technol.* 44, 860–864.
- Marti, S., Bayona, J.M., Albaiges, J., 2001. A potential source of organic pollutants into the Northeastern Atlantic: the outflow of the Mediterranean deep lying waters through the Gibraltar Strait. *Environ. Sci. Technol.* 35, 2682–2689.
- McCartney, M.S., Talley, L.D., 1982. The sub-polar mode water of the North-Atlantic ocean. *J. Phys. Oceanogr.* 12, 1169–1188.
- Munk, W., Wunsch, C., 1998. Abyssal recipes II: energetics of tidal and wind mixing. *Deep-Sea Res. Pt. I* 45, 1977–2010.
- Nizzetto, L., Lohmann, R., Gioia, R., Jahnke, A., Temme, C., Dachs, J., Herckes, P., Di Guardo, A., Jones, K.C., 2008. PAHs in air and seawater along a North-South Atlantic transect: trends, processes and possible sources. *Environ. Sci. Technol.* 42, 1580–1585.
- Osoba, W., 1999. Investigation of the free volume changes in thermally treated polyethylene by positron annihilation. *Acta Phys. Pol. A* 95, 632–636.
- Sawamura, S., 2000. Pressure dependence of the solubilities of anthracene and phenanthrene in water at 25 °C. *J. Solut. Chem.* 29, 369–375.
- Scheringer, M., Salzmann, M., Stroebe, M., Wegmann, F., Fenner, K., Hungerbühler, K., 2004. Long-range transport and global fractionation of POPs: insights from multimedia modeling studies. *Environ. Pollut.* 128, 177–188.
- Schulz, D.E., Petrick, G., Duinker, J.C., 1988. Chlorinated biphenyls in North Atlantic surface and deep water. *Mar. Pollut. Bull.* 19, 526–531.
- Schulz-Bull, D.E., Petrick, G., Bruhn, R., Duinker, J.C., 1998. Chlorobiphenyls (PCB) and PAHs in water masses of the northern North Atlantic. *Mar. Chem.* 61, 101–114.
- Semeena, S., Lammel, G., 2003. Effects of various scenarios of entry of DDT and gamma-HCH on the global environmental fate as predicted by a multi-compartment chemistry-transport model. *Fresen. Environ. Bull.* 12, 925–939.
- Siedler, G., Kuhl, A., Zenk, W., 1987. The madeira mode water. *J. Phys. Oceanogr.* 17, 1561–1570.
- Sobek, A., Gustafsson, Ö., 2004. Latitudinal fractionation of polychlorinated biphenyls in surface seawater along a 62° N – 89° N transect from the southern Norwegian Sea to the North Pole area. *Environ. Sci. Technol.* 38, 2746–2751.
- Sobek, A., Gustafsson, O., Axelman, J., 2003. An evaluation of the importance of the sampling step to the total analytical variance – a four-system field-based sampling intercomparison study for hydrophobic organic contaminants in the surface waters of the open Baltic Sea. *Int. J. Environ. Anal. Chem.* 83, 177–187.
- Stuer-Lauridsen, F., 2005. Review of passive accumulation devices for monitoring organic micropollutants in the aquatic environment. *Environ. Pollut.* 136, 503–524.
- Tomczak, M., Godfrey, J.S., 2003. *Regional Oceanography: an Introduction*, second ed. Butterworth-Heinemann, Boston (MA), pp. 1–422.
- Ullgren, J.E., van Aken, H.M., Ridderinkhof, H., de Ruijter, W.P.M., 2012. The hydrography of the Mozambique Channel from six years of continuous temperature, salinity, and velocity observations. *Deep-Sea Res. Pt. I* 69, 36–50.
- van Aken, H.M., 2001. The hydrography of the mid-latitude Northeast Atlantic Ocean – Part III: the subducted thermocline water mass. *Deep-Sea Res. Pt. I* 48, 237–267.
- van Aken, H.M., 2007. *The Oceanic Thermohaline Circulation*. Springer, New York, pp. 1–326.
- van Aken, H.M., de Jong, M.F., 2012. Hydrographic variability of Denmark strait overflow Water near cape farewell with multi-decadal to weekly time scales. *Deep-Sea Res. Pt. I* 66, 41–50.
- van Haren, H., Gostiaux, L., 2012. Energy release through internal wave breaking. *Oceanography* 25, 124–131.
- Wania, F., Mackay, D., 1995. A global distribution model for persistent organic chemicals. *Sci. Total Environ.* 160–61, 211–232.
- You, Y.Z., 1997. Seasonal variations of thermocline circulation and ventilation in the Indian Ocean. *J. Geophys. Res. Oceans* 102, 10391–10422.
- Zhou, X.Y., Zhai, L.H., Du, J.F., Han, R.D., 2000. Free volume changes in gamma-irradiated polyethylene and polytetrafluorethylene. *J. Mater. Sci. Technol.* 16, 302–304.

Supplementary data

Passive sampling of nonpolar contaminants at three deep-ocean sites

Kees Booij, Ronald van Bommel, Hendrik M. van Aken, Hans van Haren, Geert-Jan Brummer, Herman Ridderinkhof
NIOZ Royal Netherlands Institute for Sea Research, P.O. Box 59, 1790 AB Texel, The Netherlands

- S1. Effect of the triolein mass fraction on K_{sw}
- S2. Photograph and schematic drawings of the exposure cages
- S3. Amounts detected in solvent blanks, fabrication controls, and field controls, compared with the amounts detected in an average SPMD (Irminger Sea, 1.9 km depth)
- S4. Compound properties used in the modelling
- S5. SPMD-water partition coefficients
- S6. Sampler positions and bottom topography for the exposure sites
- S7. Sampling locations in Irminger Sea, Canary Basin, and Mozambique Channel
- S8. Geographical positions, water depths, exposure depths, current velocities, temperatures, salinities, and water sampling rates for the passive sampler deployments
- S9. Residuals in the retained fraction of PRCs as a function of exposure depth
- S10. Sampling rates of pyrene as a function of current speed
- S11. Aqueous concentrations of PCBs
- S12. Aqueous concentrations of PAHs, HCB, and 4,4'-DDE
- S13. Comparison of aqueous concentrations with literature values

S1. Effect of the triolein mass fraction on K_{sw}

The triolein mass fraction in the SPMDs was smaller (0.166) than intended (0.20). The reason for this was that the received LDPE lay-flat tubing had a larger wall thickness (112 μm , determined from the mass of LDPE subsamples and an adopted density of 0.91 g mL^{-1}) than requested from the manufacturer (85 μm). This was only noticed after deploying the first samplers, and we decided not to change the SPMD design for the rest of the project.

The effect of the triolein mass fraction on the SPMD-water partition coefficient (K_{sw}) can be estimated from

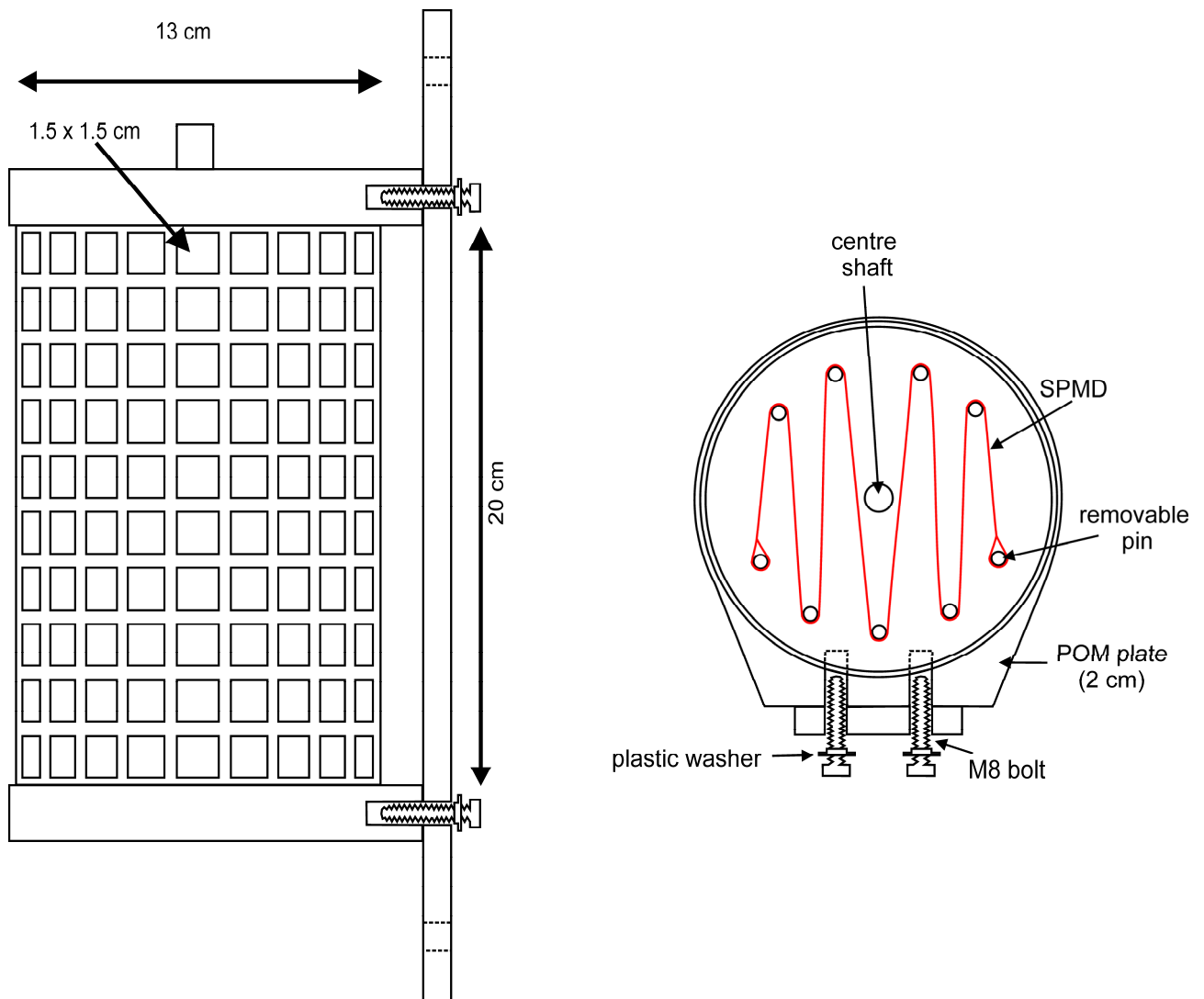
$$K_{sw} = f_t K_{tw} + (1 - f_t) K_{PE-w} \quad \text{S1-1}$$

where f_t is the mass fraction triolein, K_{tw} is the triolein-water partition coefficient, and K_{PE-w} is the LDPE-water partition coefficient. The ratio of partition coefficients for SPMDs with $f_t=0.166$ relative to standard SPMDs with $f_t=0.20$ is given by

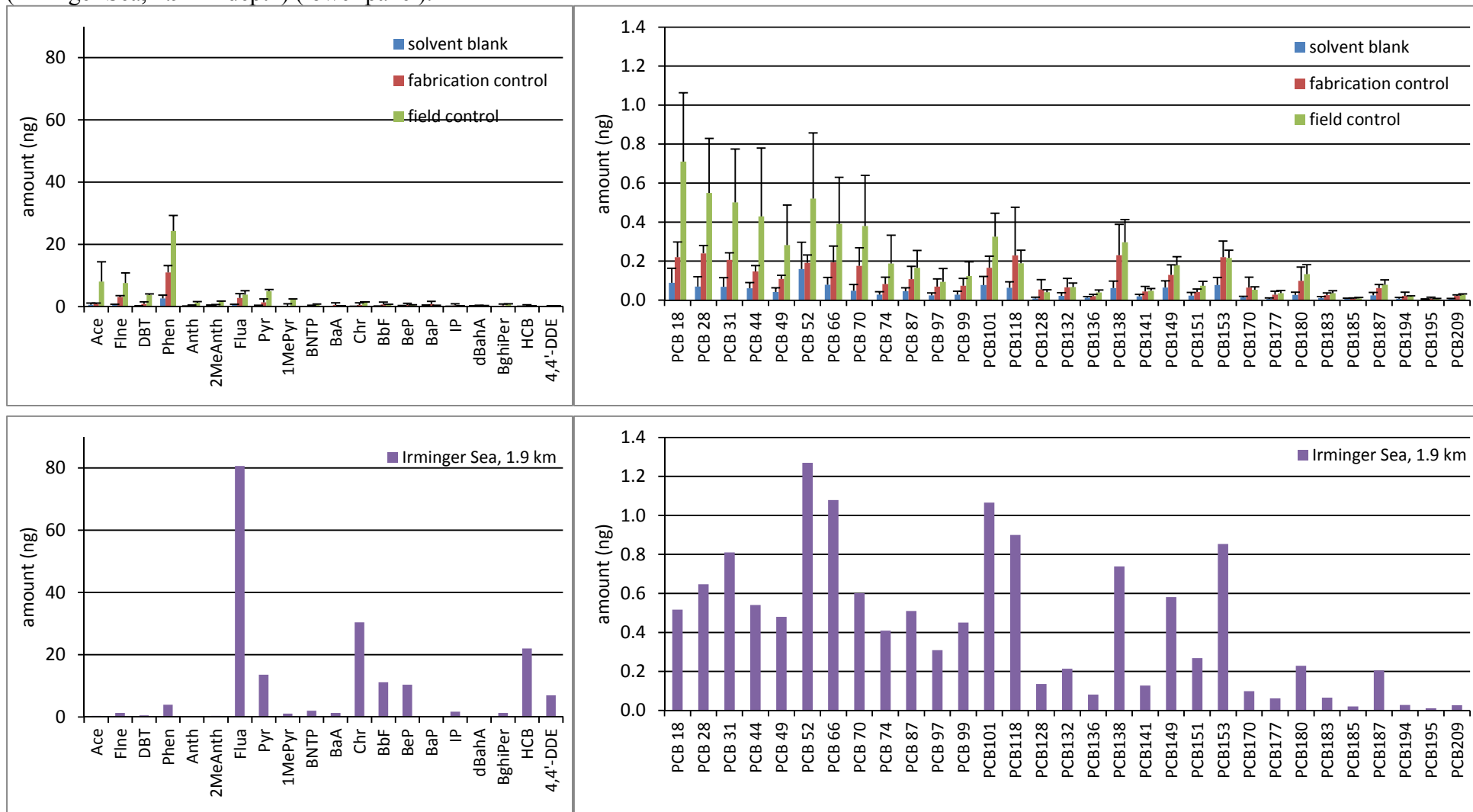
$$\frac{K_{sw,0.166}}{K_{sw,0.200}} = \frac{0.166K_{tw} + 0.834K_{PE-w}}{0.200K_{tw} + 0.800K_{PE-w}} = \frac{0.166K_{t-PE} + 0.834}{0.200K_{t-PE} + 0.800} \quad \text{S1-2}$$

where K_{t-PE} is the triolein-polyethylene partition coefficient. $\log K_{t-PE}$ values decrease from about 1.0 at $\log K_{ow} = 5$ to -0.5 at $\log K_{ow} = 8$ (supplementary data, S5). Inserting these values in eq. S1-2 yields ratios of K_{sw} values for the present study relative to those for standard SPMDs that range from 0.89 at $\log K_{ow} = 5$ to 1.03 at $\log K_{ow} = 8$. These values are sufficiently close to 1.

S2. Photograph and schematic drawings of the exposure cages.



S3. Amounts detected in solvent blanks, fabrication controls, field controls (upper panel) compared with the amounts detected in an average SPMD (Irminger Sea, 1.9 km depth) (lower panel).



S4. Compound properties used in the modelling: molar mass (MW), octanol-water partition coefficients (K_{ow}), LeBas molar volumes (V_m), LDPE-water partition coefficients (K_{PE-w}), SPMD-water partition coefficients (K_{sw}). $\log K_{sw}$ values were calculated from $\log K_{PE-w}$ when available (eq. S5-4), or alternatively from $\log K_{ow}$ (eq. S5-3).

		MW	$\log K_{ow}$	$\log K_{ow}$ source) ¹	V_m) ²	$\log K_{PE-w}$	$\log K_{PE-w}$ source) ³	$\log K_{sw}$
		(g mol ⁻¹)			(cm ³ mol ⁻¹)	(L kg ⁻¹)		(L kg ⁻¹)
Ace	acenaphthene	154.2	3.95	3	173	3.62	8	4.08
Ace-d10	acenaphthene- <i>d</i> ₁₀	164.3	3.95	4	173	3.56	8	4.03
Flne	fluorene	166.2	4.11	3	188	3.77	8	4.22
DBT	dibenzothiophene	184.3	4.38	6	191			4.18
Phen	phenanthrene	178.2	4.47	3	199	4.22	8	4.61
Phen-d10	phenanthrene- <i>d</i> ₁₀	188.3	4.47	4	199	4.15	8	4.55
Anth	anthracene	178.2	4.57	3	197	4.33	8	4.71
2MeAnth	2-methyl anthracene	192.3	5.03	6	219			4.87
Flua	fluoranthene	202.3	4.97	3	217	4.93	8	5.24
Flua-d10	fluoranthene- <i>d</i> ₁₀	212.3	4.97	4	217	4.85	8	5.17
Pyr	pyrene	202.3	5.01	3	214	5.10	8	5.39
1MePyr	1-methyl pyrene	216.3	5.48	6	236			5.34
BNTP	benzo[<i>b</i>]naphtho [2,1- <i>d</i>]thiophene	234.3	5.34	6	243			5.19
BaA	benzo[<i>a</i>]anthracene	228.3	5.83	3	248	5.73	8	5.95
Chr	chrysene (+triphenylene)	228.3	5.67	3	251	5.78	8	6.00
Chr-d12	chrysene- <i>d</i> ₁₂	240.4	5.67	4	251	5.69	8	5.92
BbF	benzo[<i>b</i>]fluoranthene	252.3	5.86	3	269	6.66	8	6.77
BeP	benzo[<i>e</i>]pyrene	252.3	5.95	5	263	6.75	10	6.85
BaP	benzo[<i>a</i>]pyrene	252.3	6.05	3	263	6.75	8	6.85
IP	indeno[1,2,3- <i>cd</i>]pyrene	276.3	6.57	3	284	7.40	8	7.43
DBahA	dibenzo[<i>a,h</i>]anthracene	278.4	6.50	5	300	7.32	8	7.36
BghiPer	benzo[<i>ghi</i>]perylene	276.3	6.63	3	277	7.27	8	7.31
HCB	hexachlorobenzene	284.8	5.64	7	221	5.43	8	5.69
4,4'-DDE	1,1-bis-(4-chlorophenyl)- 2,2-dichloroethene	318.0	6.93	7	305			6.88
PCB 4		223.1	5.23	2	226	4.19	8	4.59
PCB 18		257.5	5.67	2	247	4.90	8	5.22
PCB 28		257.5	5.66	1	247	5.40	8	5.66
PCB 29		257.5	5.65	1	247	5.31	8	5.58
PCB 31		257.5	5.78	1	247	5.30	8	5.57
PCB 44		292.0	6.11	2	268	5.48	8	5.73
PCB 49		292.0	6.11	2	268	5.67	8	5.90
PCB 52		292.0	5.95	1	268	5.55	8	5.79
PCB 66		292.0	6.11	2	268	5.95	8	6.15
PCB 70		292.0	6.11	2	268	5.85	9	6.06
PCB 74		292.0	6.11	2	268	5.85	9	6.06
PCB 87		326.4	6.55	2	289	6.18	8	6.35
PCB 97		326.4	6.55	2	289	6.10	8	6.28
PCB 99		326.4	6.55	2	289	6.38	8	6.53
PCB101		326.4	6.38	1	289	6.18	8	6.35
PCB118		326.4	6.65	1	289	6.53	8	6.66
PCB128		360.9	6.99	2	310	6.74	8	6.84
PCB132		360.9	6.99	2	310	6.60	9	6.72
PCB136		360.9	6.99	2	310	6.66	9	6.77
PCB138		360.9	7.19	1	310	6.82	8	6.92
PCB141		360.9	6.99	2	310	6.74	8	6.84
PCB149		360.9	6.99	2	310	6.59	8	6.71
PCB151		360.9	6.99	2	310	6.55	8	6.68
PCB153		360.9	6.86	1	310	6.81	8	6.91
PCB155		360.9	7.21	1	310	6.88	8	6.97
PCB170		395.3	7.43	2	331	7.25	8	7.30
PCB177		395.3	7.43	2	331	7.15	9	7.21

(continued)

S4 (continued) Compound properties used in the modelling

	<i>MW</i>	$\log K_{ow}$	$\log K_{ow}$ source) ¹	V_m) ²	$\log K_{PE-w}$	$\log K_{PE-w}$ source) ³	$\log K_{sw}$
	(g mol ⁻¹)			(cm ³ mol ⁻¹)	(L kg ⁻¹)		(L kg ⁻¹)
PCB180	395.3	7.15	1	331	7.24	8	7.29
PCB183	395.3	7.43	2	331	7.15	9	7.21
PCB185	395.3	7.43	2	331	7.15	9	7.21
PCB187	395.3	7.43	2	331	7.01	8	7.08
PCB194	429.8	7.76	1	352	7.80	9	7.78
PCB195	429.8	7.88	2	352	7.69	9	7.69
PCB204	429.8	7.88	2	352	7.77	8	7.76
PCB209	498.7	8.76	2	373	8.85	9	8.71

)¹ $\log K_{ow}$ source: 1 = Schenker et al. (2005), Final Adjusted Value, 2 = Schenker et al. (2005), calculated from $\log K_{ow} = 0.0128 MW + 2.3746$, 3 = Ma et al. (2010), Final Adjusted Value, 4 = value for the non-deuterated compound, 5 = Ma et al. (2010), calculated from $\log K_{ow} = 0.021 MW + 0.65$, 6 = US EPA (2011), 7 = Shen and Wania (2005)

)² V_m source: Huckins et al. (2006)

)³ $\log K_{PE-w}$ values from Smedes et al. (2009): 8 = experimental value, 9 = calculated from the authors' model V, 10 = value for benzo[*a*]pyrene

S5. SPMD-water partition coefficients

K_{sw} values of PRCs were determined in three separate experiments, using the cosolvent technique (Smedes et al., 2009) by incubating SPMDs for 21 d in methanol-water mixtures (mole fraction range 0 to 0.3) at ambient temperature (19 ± 1 °C) under stirring with a teflon-coated stir bar. (See Table S5-1 for details). In two experiments the analytes were spiked into the liquid phase using a solution in methanol (spike volume was 0.1% of the liquid volume). In one experiment the analytes were spiked into the triolein by evaporating a solution in 2,2,4-trimethylpentane to dryness, using a stream of nitrogen gas, and re-dissolving the analytes in triolein. After the incubation the liquid phase was transferred to a separation funnel. The methanol concentration was reduced to <20% by adding ultrapure water. The resulting mixture was extracted twice with 100 mL pentane. SPMDs were wiped dry with a paper tissue, and dialysed twice (16 h and 24 h) with 50 mL pentane. Appropriate subsamples were taken from the extracts to bring the final concentrations within the calibrated range of the analytical equipment. Extracts were cleaned-up with silica (2 g, deactivated with 6% water, elution with pentane), and were analysed by GC-ECD (PCB29, PCB155, PCB204) and by GC-MS (PCB4 and deuterated PAHs).

The logarithms of K_{sw} ($L\ kg^{-1}$) were obtained by linear regression, using the model

$$\log\left(\frac{K_{sm}}{V_m}\right) = \log\left(\frac{K_{sw}}{V_w}\right) - a x \quad S5-1$$

where K_{sm} is the sampler-mixture partition coefficient, V_m is the molar volume of the mixture (assuming conservative mixing), V_w is the molar volume of water, x is the mole fraction methanol, and a is a constant (Smedes et al., 2009).

Additional values of $\log K_{sw}$ were calculated from triolein-water partition (K_{tw}) coefficients reported by Chiou (1985) and by Jabusch and Swackhamer (2005) and LDPE-water partition (K_{PE-w}) coefficients from Smedes et al. (2009). K_{tw} values in volume per volume units were divided by the triolein density ($0.91\ kg\ L^{-1}$) to obtain K_{tw} in volume per mass units.

$$K_{sw} = f_t K_{tw} + (1 - f_t) K_{PE-w} \quad S5-2$$

where f_t is the triolein mass fraction, K_{tw} is the lipid-water partition coefficient, and K_{PE-w} is the LDPE-water partition coefficient.

Experimental $\log K_{sw}$ values from the present study are similar to the values that are calculated from $\log K_{tw}$ and $\log K_{PE-w}$ (Fig. S5-1). Experimental and calculated $\log K_{sw}$ values were modelled as a linear function of $\log K_{ow}$ and $\log K_{PE-w}$

$$\log K_{sw} = 1.057 \log K_{ow} - 0.45 \quad S5-3$$

$s = 0.30, R^2 = 0.95$

$$\log K_{sw} = 0.885 \log K_{PE-w} + 0.88 \quad S5-4$$

$s = 0.17, R^2 = 0.98$

These results suggest that $\log K_{PE-w}$ is a better descriptor of $\log K_{sw}$ than $\log K_{ow}$ (standard errors of 0.17 and 0.30, respectively). In cases where $\log K_{PE-w}$ are not available, the less accurate relationship with $\log K_{ow}$ may be used.

Table S5-1. Summary of experimental conditions of three determinations of SPMD-water partition coefficients.

experiment	k40-44	k45-49	k50-54
SPMD mass (g)	2.41	0.34	2.57
mixture volume (L)	2.00	0.20	2.00
spike added to	mixture	mixture	SPMD
incubation time (d)	22	22	20

Table S5-2. Experimental values of SPMD-water partition coefficients

experiment	$\log K_{ow}$		k40-44	k45-49	k50-54	average	s
		source) ¹	$\log K_{sw}$	$\log K_{sw}$	$\log K_{sw}$		
			(L kg ⁻¹)	(L kg ⁻¹)	(L kg ⁻¹)		
PCB 4	5.23	2	4.76	4.61	4.81	4.73	0.10
PCB 29	5.65	1	5.89	5.65	5.90	5.81	0.14
PCB155	7.21	1	6.98	6.87	7.24	7.03	0.19
PCB204	2.45	2	7.56	7.34	7.58	7.49	0.13
Acenaphthene- <i>d</i> ₁₀	3.95	3	4.02	3.83	4.05	3.97	0.12
Phenanthrene- <i>d</i> ₁₀	4.47	3	4.47	4.43	4.54	4.48	0.06
Fluoranthene- <i>d</i> ₁₀	4.97	3	5.09	4.98	5.09	5.05	0.06
Chrysene- <i>d</i> ₁₂	5.67	3	5.76	5.67	5.85	5.76	0.09

¹ 1 = Schenker et al. (2005), Final Adjusted Value , 2 = Schenker et al. (2005), calculated from $\log K_{ow} = 0.0128 MW + 2.3746$, 3 = Ma et al. (2010), Final Adjusted Value of the non-deuterated compound.

Table S5-3. SPMD-water partition coefficients calculated from triolein-water partition coefficients from Jabusch and Swackhamer (2005) and LDPE-water partition coefficients (K_{PE-w}) from Smedes et al. (2009).

	$\log K_{ow}$	$\log K_{ow}$	$\log K_{tw}$	$\log K_{tw}$	$\log K_{PE-w}$	$\log K_{sw}$
		source) ¹	(L L ⁻¹)	(L kg ⁻¹)	(L kg ⁻¹)	(L kg ⁻¹)
PCB1	4.61	2	4.90	4.94	3.72	4.34
PCB8	5.11	1	5.70	5.74	4.65	5.16
PCB52	5.95	1	5.71	5.75	5.55	5.60
PCB54	6.11	2	5.97	6.01	5.39	5.60
PCB61	6.14	1	6.44	6.48	5.85	6.07
PCB77	6.11	2	7.06	7.10	6.08	6.54
PCB126	6.55	2	7.60	7.64	6.56	7.07
PCB128	6.99	2	7.24	7.28	6.74	6.91
PCB155	7.21	1	7.10	7.14	6.88	6.95
PCB169	6.99	2	7.65	7.69	7.05	7.27
PCB194	7.88	2	8.10	8.14	7.80	7.89
PCB209	8.32	2	8.30	8.34	8.85	8.79

¹ 1 = Schenker et al. (2005), Final Adjusted Value , 2= Schenker et al. (2005), calculated from $\log K_{ow} = 0.0128 MW + 2.3746$.

Table S5-3. SPMD-water partition coefficients calculated from triolein-water partition coefficients from Chiou (1985) and LDPE-water partition coefficients (K_{PE-w}) from Smedes et al. (2009).

	$\log K_{ow}$	$\log K_{ow}$ source) ¹	$\log K_{tw}$ (L L ⁻¹)	$\log K_{tw}$ (L kg ⁻¹)	$\log K_{PE-w}$ (L kg ⁻¹)	$\log K_{sw}$ (L kg ⁻¹)
biphenyl	3.88	1	4.37	4.41	3.23	3.81
PCB 1	4.79	2	4.77	4.81	3.72	4.23
PCB 4	5.23	2	5.05	5.09	4.2	4.57
PCB 8	5.11	1	5.30	5.34	4.65	4.90
PCB 15	5.35	1	5.48	5.52	5.1	5.22
PCB 28	5.66	1	5.52	5.56	5.4	5.44
PCB 52	5.95	1	5.62	5.66	5.55	5.57
PCB101	6.38	1	5.81	5.85	6.18	6.13
PCB153	6.86	1	6.23	6.27	6.81	6.74

¹ 1 = Schenker et al. (2005), Final Adjusted Value, 2 = Schenker et al. (2005), calculated from $\log K_{ow} = 0.0128 MW + 2.3746$.

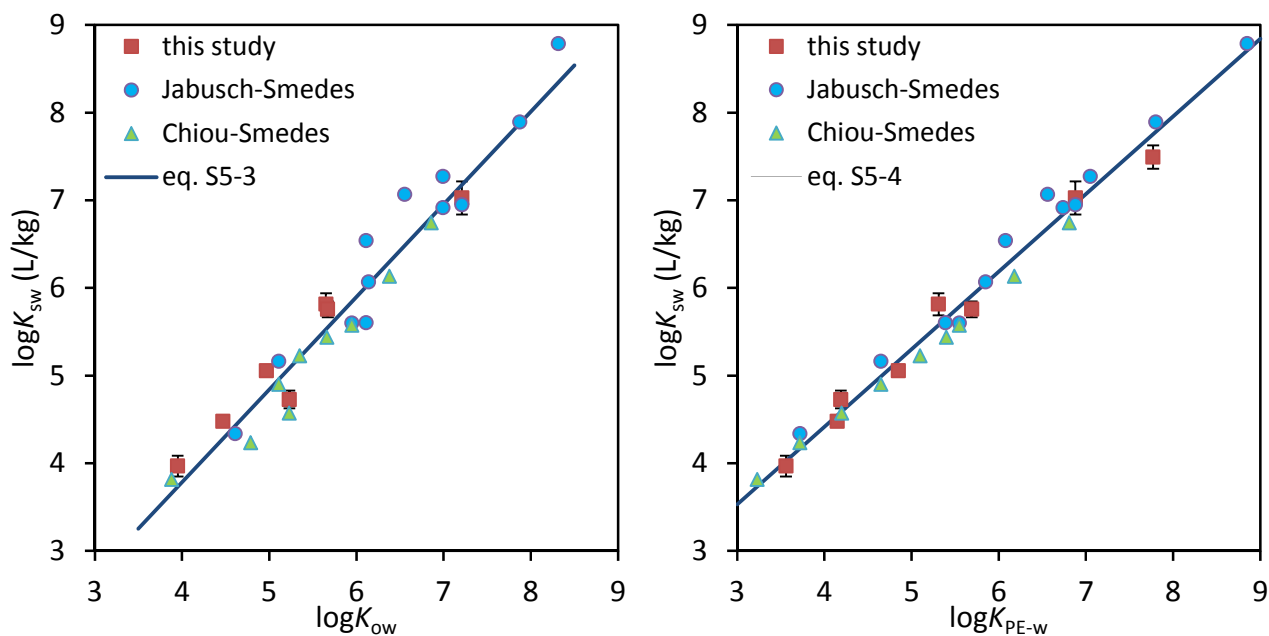
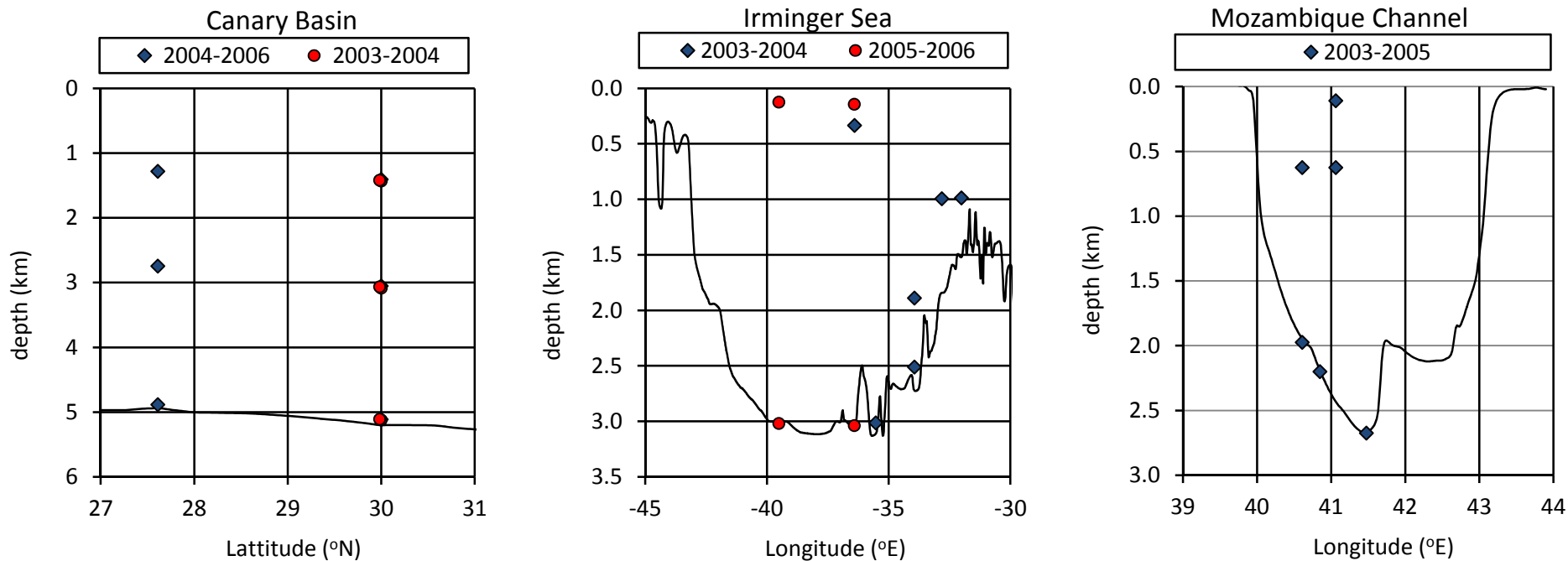


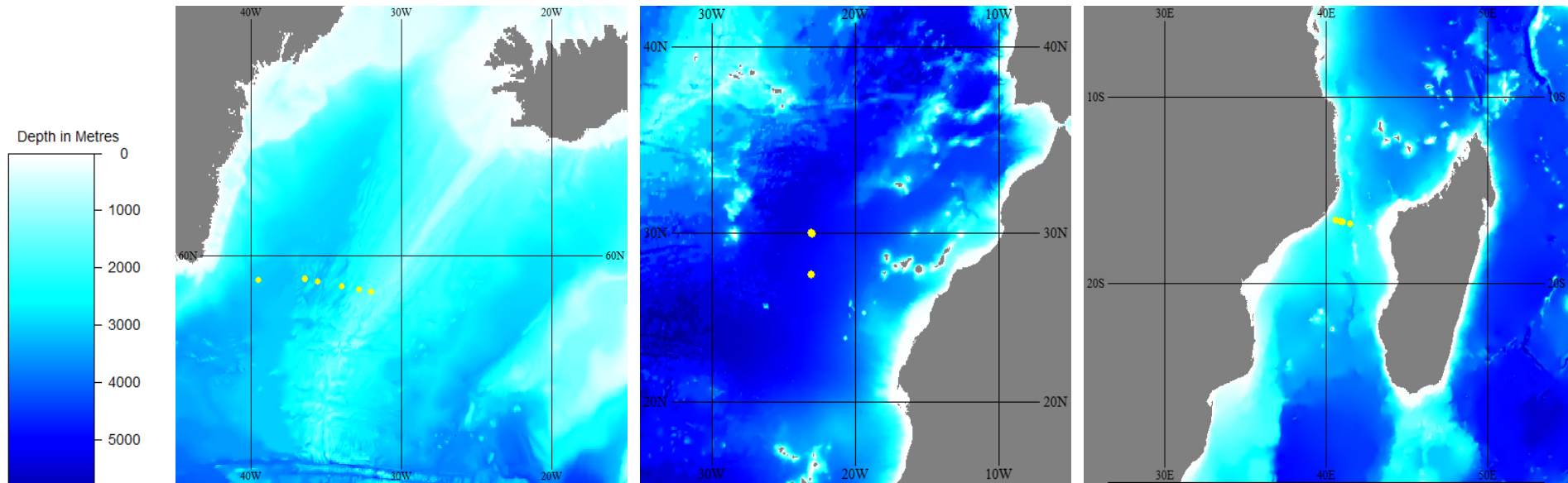
Figure S5-1. Logarithms of SPMD-water partition coefficients as a function of $\log K_{ow}$ (left) and $\log K_{PE-w}$ (right).

S6. Sampler positions and bottom topography)^a for the sites in the Canary Basin (~ 23.1 °W), Irminger Sea (~ 59.1 °N), and the Mozambique Channel (~ 16.7 °S).



^a Obtained by interpolation from the GEBCO One Minute Grid, version 2.0, <http://www.gebco.net>

S7. Sampling locations (yellow circles) in the Irminger Sea (left), the Canary Basin (middle), and the Mozambique Channel (right).)^a

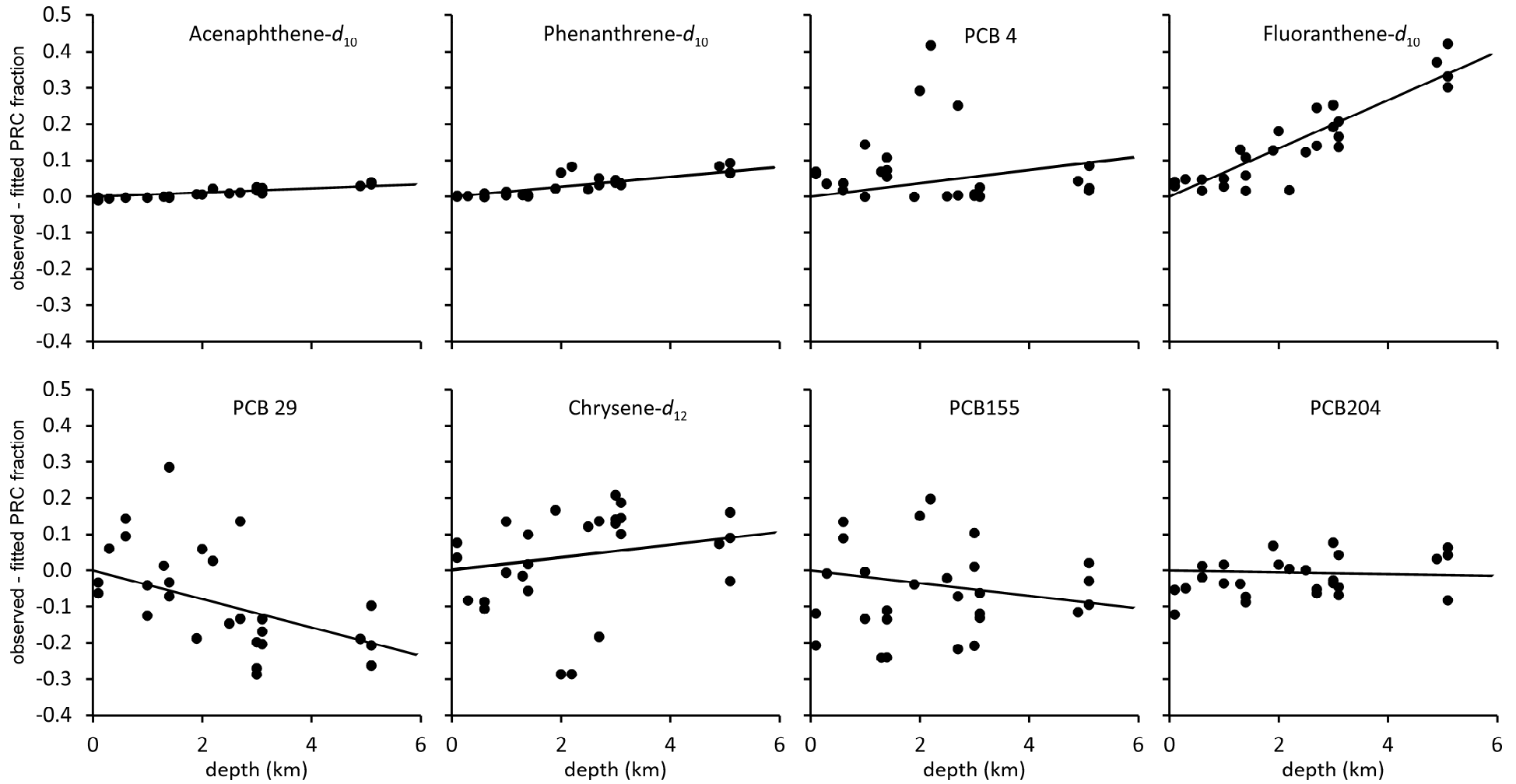


)^a Obtained from the GEBCO One Minute Grid, version 2.0, <http://www.gebco.net>

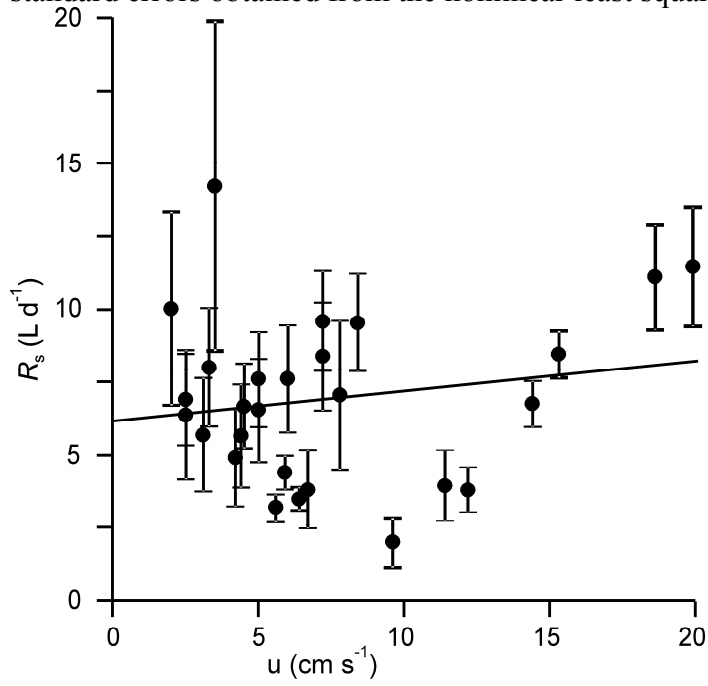
S8. Geographical positions, water depths, exposure depths, current velocities, temperatures, salinities, and sampling rates of pyrene for the passive sampler deployments. Uncertainties represent standard errors.

Mooring ID	latitude (°N)	longitude (°E)	water depth (km)	sampler depth (km)	deployment date (yyyy/mm/dd)	recovery date (yyyy/mm/dd)	exposure time (d)	U (cm s ⁻¹)	temperature (°C)	salinity	<i>R_s</i> of pyrene (L d ⁻¹)
Canary Basin											
LOCO12	30.000	-23.076	5.1	1.4	2003/03/14	2004/10/16	582	5.6 ± 3.1	6.6 ± 0.2	35.3	3.2 ± 0.5
LOCO12	30.000	-23.076	5.1	3.1	2003/03/14	2004/10/16	582	5.0 ± 2.7	2.8 ± 0.1	34.9	7.6 ± 1.6
LOCO12	30.000	-23.076	5.1	5.1	2003/03/14	2004/10/16	582	4.2 ± 2.3	2.4 ± 0.0	34.9	4.9 ± 1.7
LOCO13	29.983	-23.022	5.1	1.4	2003/03/14	2004/10/18	584	5.9 ± 3.2	3.6 ± 0.1	35.3	4.4 ± 0.6
LOCO13	29.983	-23.022	5.1	3.1	2003/03/14	2004/10/18	584	5.0 ± 2.7	2.7 ± 0.0	34.9	6.5 ± 1.7
LOCO13	29.983	-23.022	5.1	5.1	2003/03/14	2004/10/18	584	4.4 ± 2.3	2.3 ± 0.0	34.9	5.7 ± 1.8
LOCO12/2	30.001	-23.054	5.1	1.4	2004/10/17	2006/05/19	579	3.5 ± 2.0	5.9 ± 0.2	35.3	14.2 ± 5.7
LOCO12/2	30.001	-23.054	5.1	3.1	2004/10/17	2006/05/19	579	2.5 ± 1.3	2.7 ± 0.0	34.9	6.9 ± 1.6
LOCO12/2	30.001	-23.054	5.1	5.1	2004/10/17	2006/05/19	579	2.5 ± 1.4	2.4 ± 0.0	34.9	6.4 ± 2.2
LOCO13/2	27.613	-23.066	4.9	1.3	2004/10/25	2006/05/26	578	4.5 ± 2.5	6.1 ± 0.1	35.3	6.7 ± 1.5
LOCO13/2	27.613	-23.066	4.9	2.7	2004/10/25	2006/05/26	578	3.3 ± 1.8	2.7 ± 0.0	34.9	8.0 ± 2.0
LOCO13/2	27.613	-23.066	4.9	4.9	2004/10/25	2006/05/26	578	3.1 ± 1.6	2.4 ± 0.0	34.9	5.7 ± 1.9
Irminger Sea											
LOCO03-1	59.237	-36.397	3.0	0.3	2003/08/28	2004/10/05	404	15.3 ± 8.4	6.5 ± 0.7	34.9	8.5 ± 0.8
LOCO15-1	59.145	-35.526	3.0	3.0	2003/08/27	2004/10/06	406	6.0 ± 3.6	3.6 ± 0.2	34.9	7.6 ± 1.8
LOCO16-1	58.995	-33.935	2.5	1.9	2003/08/27	2004/10/06	406	7.2 ± 4.0	3.2 ± 0.1	34.9	8.4 ± 1.9
LOCO16-1	58.995	-33.935	2.5	2.5	2003/08/27	2004/10/06	406	8.4 ± 6.2	2.9 ± 0.1	34.9	9.5 ± 1.7
LOCO17-1	58.889	-32.808	2.0	1.0	2003/08/26	2004/10/07	408	6.4 ± 3.6	4.2 ± 0.3	34.9	3.5 ± 0.4
LOCO18-1	58.812	-31.997	1.5	1.0	2003/08/26	2004/10/07	408	7.2 ± 3.8	4.1 ± 0.2	34.9	9.6 ± 1.7
LOCO02-3	59.203	-39.508	3.0	0.1	2005/09/15	2006/08/24	343	12.2 ± 6.5	5.2 ± 0.0	35.0	3.8 ± 0.8
LOCO02-3	59.203	-39.508	3.0	3.0	2005/09/15	2006/08/24	343	11.4 ± 5.6	1.2 ± 0.0	34.9	3.9 ± 1.2
LOCO03-3	59.248	-36.568	3.0	0.1	2005/09/14	2006/08/28	348	14.4 ± 7.5	6.0 ± 0.0	35.0	6.7 ± 0.8
LOCO03-3	59.248	-36.568	3.0	3.0	2005/09/14	2006/08/28	348	7.8 ± 4.0	2.1 ± 0.0	34.9	7.1 ± 2.5
Mozambique Channel											
LMC 5A	-16.766	41.066	2.4	0.1	2003/11/20	2005/03/04	470	49.4 ± 40.7	11.6 ± 0.8	35.0	
LMC 5A	-16.766	41.066	2.4	0.6	2003/11/20	2005/03/04	470	18.6 ± 11.3	11.6 ± 0.8	35.0	11.1 ± 1.8
LMC 5	-16.646	40.612	2.0	0.6	2003/11/21	2005/03/03	468	19.9 ± 11.1	9.1 ± 0.5	34.8	11.5 ± 2.1
LMC 5	-16.646	40.612	2.0	2.0	2003/11/21	2005/03/03	468	6.7 ± 4.0	2.6 ± 0.1	34.8	3.8 ± 1.4
ST	-16.714	40.852	2.2	2.2	2003/11/22	2005/03/04	468	9.6 ± 5.3	2.4 ± 0.1	34.8	2.0 ± 0.8
LMC 6	-16.870	41.479	2.7	2.7	2003/11/19	2005/03/05	472	2.0 ± 30.8	2.1 ± 0.1	34.8	10.0 ± 3.3

S9. Residuals in the retained fraction of PRCs as a function of exposure depth.



S10. Sampling rates of pyrene as a function of average current speed. Error bars represent the standard errors obtained from the nonlinear least squares analysis of the PRC dissipation data.



S11. (continued) Aqueous concentrations of PCBs (pg L⁻¹). nd: < LOD

Mooring ID	sampler depth (km)	PCB 136	PCB 138	PCB 141	PCB 149	PCB 151	PCB 153	PCB 170	PCB 177	PCB 180	PCB 183	PCB 185	PCB 187	PCB 194	PCB 195	PCB 209
LOD		0.01	0.12	0.01	0.05	0.02	0.04	0.02	0.01	0.05	0.01	0.01	0.03	0.005	0.003	0.005
Canary Basin																
LOCO12	1.4	0.11	1.1	0.15	0.59	0.24	0.84	0.20	0.11	0.29	0.08	0.02	0.27	0.030	0.020	nd
LOCO12	3.1	nd	0.10	0.02	0.07	0.03	0.14	0.03	0.01	0.06	nd	0.00	0.04	0.009	0.004	nd
LOCO12	5.1	nd	0.45	0.08	0.12	0.04	0.26	0.16	0.04	0.19	0.03	0.01	0.06	0.030	0.016	nd
LOCO13	1.4	0.08	0.77	0.10	0.42	0.12	0.61	0.10	0.08	0.19	0.06	0.01	0.20	nd	0.007	nd
LOCO13	3.1	nd	0.13	0.02	0.07	0.04	0.12	0.03	0.02	0.06	0.01	nd	0.05	0.009	0.005	nd
LOCO13	5.1	nd	0.003	nd												
LOCO12/2	1.4	0.01	0.21	0.01	0.08	0.03	0.11	0.02	0.02	0.03	0.01	0.01	0.06	nd	0.003	nd
LOCO12/2	3.1	nd	0.13	nd	nd	0.03	0.06	0.02	0.02	0.05	0.02	nd	0.06	0.008	0.004	nd
LOCO12/2	5.1	nd														
LOCO13/2	1.3	0.05	0.32	0.03	0.15	0.09	0.19	0.02	0.03	0.05	0.02	0.01	0.10	nd	nd	nd
LOCO13/2	2.7	nd	0.13	nd	0.04	0.03	0.06	0.02	0.02	0.05	0.02	nd	0.06	0.004	0.003	nd
LOCO13/2	4.9	nd	0.02	nd	nd	nd	nd	nd								
Irminger Sea																
LOCO03-1	0.3	0.01	nd	nd	0.08	0.04	0.11	nd								
LOCO15-1	3.0	0.02	0.25	0.03	0.15	0.06	0.23	0.04	0.02	0.06	0.02	nd	0.07	0.013	0.004	nd
LOCO16-1	1.9	0.01	0.15	0.03	0.14	0.07	0.22	0.02	nd	nd	nd	nd	0.04	nd	nd	nd
LOCO16-1	2.5	0.02	0.20	0.03	0.14	0.07	0.21	0.03	0.01	0.05	0.01	nd	0.05	0.007	0.003	nd
LOCO17-1	1.0	0.05	nd	0.05	0.29	0.13	0.39	nd	nd	nd	nd	nd	0.09	nd	nd	nd
LOCO18-1	1.0	0.01	0.12	0.01	0.11	0.05	0.14	nd	nd	nd	nd	nd	0.03	nd	nd	nd
LOCO02-3	0.1	nd	nd	nd	nd	0.09	0.12	nd								
LOCO02-3	3.0	0.05	0.35	0.06	0.17	0.19	0.46	nd	nd	nd	nd	nd	0.10	0.013	nd	nd
LOCO03-3	0.1	0.02	nd	nd	nd	nd	0.10	nd								
LOCO03-3	3.0	0.03	0.25	0.02	0.12	0.08	0.18	nd	nd	nd	0.02	nd	0.08	nd	nd	nd
Mozambique Channel																
LMC 5A	0.6	nd	nd	nd	nd	0.02	nd									
LMC 5	0.6	nd	nd	nd	nd	0.02	nd									
LMC 5	2.0	nd	nd	nd	nd	nd	nd	0.04	nd							
ST	2.2	nd	nd	nd	nd	nd	nd	0.07	nd							
LMC 6	2.7	nd	nd	nd	nd	nd	nd	0.02	nd	nd	nd	nd	nd	nd	0.002	nd

S12. (continued) Aqueous concentrations of PAHs, HCB, and 4,4'-DDE (pg L⁻¹). nd: < LOD

Mooring ID	sampler depth (km)	1MePyr	BNTF	BaA	Chr	BbF	BeP	BaP	IP	dBahA	BghiPer
LOD		0.4	0.3	0.05	0.1	0.2	0.1	0.2	0.1	0.1	0.1
Canary Basin											
LOCO12	1.4	0.6	4.5	6.9	50	8.9	8.8	6.2	4.4	1.3	3.6
LOCO12	3.1	nd	2.9	4.0	6.8	5.8	6.1	3.8	2.8	0.7	2.3
LOCO12	5.1	nd	nd	0.33	2.5	0.9	1.1	0.3	0.2	nd	nd
LOCO13	1.4	0.5	2.8	1.3	27	2.7	3.5	1.2	1.1	0.2	0.7
LOCO13	3.1	nd	0.3	0.04	4.6	1.6	2.8	nd	0.1	nd	nd
LOCO13	5.1	nd	nd	nd	1.5	0.9	0.6	0.8	nd	nd	nd
LOCO12/2	1.4	nd	1.2	nd	13	0.8	1.1	nd	nd	nd	nd
LOCO12/2	3.1	nd	0.4	nd	3.6	2.0	2.8	nd	0.2	nd	nd
LOCO12/2	5.1	nd	nd	nd	1.4	0.3	0.5	nd	nd	nd	nd
LOCO13/2	1.3	nd	1.7	nd	16	0.6	1.1	nd	nd	nd	nd
LOCO13/2	2.7	nd	0.5	nd	4.6	1.8	2.7	nd	0.1	nd	nd
LOCO13/2	4.9	nd	nd	nd	1.9	0.6	0.9	nd	nd	nd	nd
Irminger Sea											
LOCO03-1	0.3	nd	1.5	0.13	8.9	2.2	1.1	0.3	0.4	nd	nd
LOCO15-1	3.0	nd	1.2	0.53	9.7	3.7	3.3	nd	0.4	nd	0.2
LOCO16-1	1.9	nd	1.2	0.38	11	3.5	3.2	nd	0.5	nd	0.2
LOCO16-1	2.5	nd	1.5	0.34	9.9	2.8	2.6	nd	0.4	nd	nd
LOCO17-1	1.0	nd	1.7	0.86	29	5.9	4.3	nd	0.9	nd	nd
LOCO18-1	1.0	nd	1.6	0.25	11	2.3	1.7	0.2	0.3	nd	0.1
LOCO02-3	0.1	nd	2.2	0.36	22	6.1	3.2	0.5	0.6	nd	0.2
LOCO02-3	3.0	2.1	6.4	4.9	26	15	8.7	1.9	2.0	0.4	1.3
LOCO03-3	0.1	nd	1.7	0.24	13	3.0	1.5	nd	0.3	nd	0.2
LOCO03-3	3.0	0.6	2.7	1.7	15	7.3	4.5	0.6	0.8	0.2	0.6
Mozambique Channel											
LMC 5A	0.6	nd	nd	nd	0.4	nd	nd	nd	nd	nd	nd
LMC 5	0.6	nd	nd	nd	0.4	nd	nd	nd	nd	nd	nd
LMC 5	2.0	nd	nd	nd	0.8	nd	nd	nd	nd	nd	nd
ST	2.2	nd	nd	nd	2.2	0.6	0.8	nd	nd	nd	nd
LMC 6	2.7	nd	nd	nd	0.3	nd	nd	nd	nd	nd	nd

S13. Comparison of aqueous concentrations with literature values.

Fluoranthene concentrations in the Irminger Sea (75 pg L^{-1}) and the Canary Basin at 1.4 km (130 pg L^{-1}) are similar to literature values for the East and West Atlantic Ocean, the Norwegian Sea and the area around Fram Strait (Table 1), with the exception of values of <5 to 9 pg L^{-1} reported for locations north and south of the Iceland-Faroe-Scotland Ridge (Schulz-Bull et al., 1998).

Fluoranthene concentrations in the Mozambique Channel at 0.6 km were $< 3 \text{ pg L}^{-1}$, but we found no literature values to compare this with.

Concentrations of PCB153 in the Irminger Sea (0.2 pg L^{-1}) and the near-surface layers in the Canary Basin (0.4 pg L^{-1}) are higher than the concentrations reported for the Iceland-Faroe-Scotland Ridge area (0.02 - 0.06 pg L^{-1}) (Schulz-Bull et al., 1998), and the Norwegian Sea and Fram Strait ($< 0.01 \text{ pg L}^{-1}$) (Gioia et al., 2008), but are similar to the concentrations reported by Sobek and Gustafsson (2004) for the Norwegian Sea and the Barents Sea (0.2 - 0.4 pg L^{-1}). PCB153 was not detected in the Mozambique Channel ($<0.04 \text{ pg L}^{-1}$) whereas Iwata et al. (1993) report concentrations of 0.2 - 0.8 pg L^{-1} for Indian Ocean surface waters.

Concentrations of 4,4'-DDE in the Irminger Sea (2.5 pg L^{-1}) and the Canary Basin at 1.4 km (7 pg L^{-1}) are higher than previous SPMD based values from the East Atlantic (0.3 - 1.4) and batch sampling based concentrations from the North Atlantic (0.1 - 0.5 pg L^{-1}). DDE concentrations in the Mozambique Channel ($\sim 1 \text{ pg L}^{-1}$) are similar to those reported by Iwata et al. (1993) for the Arabian Sea, the Bay of Bengal, and the Eastern Indian Ocean (0.4 - 5 pg L^{-1}).

HCB concentrations in the Irminger Sea (12 pg L^{-1}) are similar to values observed in the Arctic Ocean (7 - 19 pg L^{-1}) (Barber et al., 2005) and the region near Fram Strait (2 - 10 pg L^{-1}) (Lohmann et al., 2009), but the latter authors observed lower concentrations in the Norwegian Sea (1 - 2 pg L^{-1}). HCB concentrations in the Canary Basin at 1.4 km (5 pg L^{-1}) were similar to earlier SPMD based values for East Atlantic surface water (2 - 9 pg L^{-1}) (Booij et al., 2007), but higher than batch sampling based concentrations in off shore North Atlantic surface water between Rhode Island and the equator (0.1 - 1 pg L^{-1}). HCB concentrations of 4 pg L^{-1} at 0.6 km in the Mozambique Channel seems to be high, but to our knowledge there are no literature values from the Indian Ocean available for comparison. However, Gioia et al. (2012) report concentrations of atmospheric HCB to be similar in the Indian Ocean (1 - 54 pg m^{-3}) and the Eastern Atlantic Ocean between 13°N and 31°S (1 - 22 pg m^{-3}). This suggests that HCB concentrations in surface waters of these oceans could also be similar, which is in line with our estimates for the Canary Basin (1.4 km) and the Mozambique Channel (0.6 km).

References

- Barber, J.L., Sweetman, A.J., van Wijk, D., Jones, K.C., 2005. Hexachlorobenzene in the global environment: emissions, levels, distribution, trends and processes. *Sci. Total Environ.* 349, 1-44.
- Booij, K., van Bommel, R., Jones, K.C., Barber, J.L., 2007. Air-water distribution of hexachlorobenzene and 4,4'-DDE along a North-South Atlantic transect. *Mar. Pollut. Bull.* 54, 814-819.
- Chiou, C.T., 1985. Partition coefficients of organic compounds in lipid-water systems and correlations with fish bioconcentration factors. *Environ. Sci. Technol.* 19, 57-62.
- Gioia, R., Li, J., Schuster, J., Zhang, Y.L., Zhang, G., Li, X.D., Spiro, B., Bhatia, R.S., Dachs, J., Jones, K.C., 2012. Factors Affecting the Occurrence and Transport of Atmospheric Organochlorines in the China Sea and the Northern Indian and South East Atlantic Oceans. *Environ. Sci. Technol.* 46, 10012-10021.

- Gioia, R., Lohmann, R., Dachs, J., Temme, C., Lakaschus, S., Schulz-Bull, D., Hand, I., Jones, K.C., 2008. Polychlorinated biphenyls in air and water of the North Atlantic and Arctic Ocean. *J. Geophys. Res. -Atmos.* 113, D19302
- Huckins, J.N., Petty, J.D., Booij, K., 2006. *Monitors of Organic Chemicals in the Environment: Semipermeable Membrane Devices*. Springer, New York, pp. 1-223
- Iwata, H., Tanabe, S., Sakai, N., Tatsukawa, R., 1993. Distribution of persistent organochlorines in the oceanic air and surface seawater and the role of ocean on their global transport and fate. *Environ. Sci. Technol.* 27, 1080-1098.
- Jabusch, T.W., Swackhamer, D.L., 2005. Partitioning of polychlorinated biphenyls in octanol/water, triolein/water, and membrane/water systems. *Chemosphere* 60, 1270-1278.
- Lohmann, R., Gioia, R., Jones, K.C., Nizzetto, L., Temme, C., Xie, Z., Schulz-Bull, D., Hand, I., Morgan, E., Jantunen, L., 2009. Organochlorine pesticides and PAHs in the surface water and atmosphere of the North Atlantic and Arctic Ocean. *Environ. Sci. Technol.* 43, 5633-5639.
- Ma, Y.G., Lei, Y.D., Xiao, H., Wania, F., Wang, W.H., 2010. Critical review and recommended values for the physical chemical property data of 15 polycyclic aromatic hydrocarbons at 25 degrees C. *J. Chem. Eng. Data* 55, 819-825.
- Schenker, U., MacLeod, M., Scheringer, M., Hungerbuhler, K., 2005. Improving data quality for environmental fate models: A least-squares adjustment procedure for harmonizing physicochemical properties of organic compounds. *Environ. Sci. Technol.* 39, 8434-8441.
- Schulz-Bull, D.E., Petrick, G., Bruhn, R., Duinker, J.C., 1998. Chlorobiphenyls (PCB) and PAHs in water masses of the northern North Atlantic. *Mar. Chem.* 61, 101-114.
- Shen, L., Wania, F., 2005. Compilation, evaluation, and selection of physical-chemical property data for organochlorine pesticides. *J. Chem. Eng. Data* 50, 742-768.
- Smedes, F., Geertsma, R.W., van der Zande, T., Booij, K., 2009. Polymer-water partition coefficients of hydrophobic compounds for passive sampling: application of cosolvent models for validation. *Environ. Sci. Technol.* 43, 7047-7054.
- Sobek, A., Gustafsson, Ö., 2004. Latitudinal fractionation of polychlorinated biphenyls in surface seawater along a 62° N - 89° N transect from the southern Norwegian Sea to the North Pole area. *Environ. Sci. Technol.* 38, 2746-2751.
- US EPA, 2011. Estimation Program Interface (EPI) Suite. U.S. Environmental Protection Agency. <http://www.epa.gov/opptintr/exposure/pubs/episuitedl.htm>